Universität Ulm
Fakultät für Informatik

Interaction of ON and OFF Pathways for Visual Contrast Measurement

Heiko Neumann, Thorsten Hansen
Universität Ulm
Luiz Pessoa
Universidade Federal do Rio de Janeiro

Nr. 98-07
Ulmer Informatik-Berichte
Juni 1998

Interaction of ON and OFF Pathways for Visual Contrast Measurement[1]

Heiko Neumann†, Luiz Pessoa‡, Thorsten Hansen†[2]

†Universität Ulm,
Fakultät für Informatik, Abteilung Neuroinformatik,
Oberer Eselsberg, D-89069 Ulm, Germany

‡Universidade Federal do Rio de Janeiro,
Programa de Engenharia de Sistemas e Computação – COPPE Sistemas,
Ilha do Fundão, Rio de Janeiro, RJ 21945-970, Brazil

Abstract

We propose a novel model of visual contrast measurement based on segregated ON and OFF pathways. Two driving forces have shaped our investigation: (1) establishing a mechanism selective for sharp local transitions in the luminance distribution; and (2) generating a robust scheme of oriented contrast detection. Our starting point was the architecture of early stages in the mammalian visual system. We show that the circuit behaves as a *soft AND-gate* and analyze the scale-space selectivity properties of the model in detail. The theoretical analysis is supplemented by computer simulations in which we selectively investigate key functionalities of the proposed contrast detection scheme. We demonstrate that the model is capable of successfully processing synthetic as well as natural images, thus illustrating the potential of the method for computer vision applications.

1 Introduction

An important goal of computer and biological vision processing mechanisms is the robust and reliable detection of local contrast information present in the luminance distribution. A discontinuity in a visual stimulus signals a causally related change in at least one physical scene parameter (Marr, 1982). Discontinuities are of equal importance for artificial and biological vision systems as they allow for robust estimation of, e.g., optical flow and local stereoscopic disparity information. They also support robust object recognition and pose estimation.

In many cases, the search for designing optimal filters to detect discontinuities has been influenced by neurophysiological investigations concerning the shape of receptive field (RF) profiles of cortical neurons tuned to oriented contrast. A lot of effort was devoted to describing the formal properties of families of filters designed to detect local structure (such as contrast edges) and whether they are capable of coding visual information in an optimal manner. Marr and Hildreth (1980) proposed that early mechanisms in the visual system implement an isotropic 2nd order derivative filtering stage and model these by Laplacian of circular symmetric Gaussians. As Marr (1982) pointed out, such filters closely resemble the RF profile of retinal ganglion cells. More recently, image processing filters built from Gabor or Gaussian derivative functions have been commonly employed (Daugman, 1985; Koenderink and van Doorn, 1990). Such families of oriented filters sample the image such that the contents can be restored with minimal loss of information and have been linked to the RF structure of cells at early levels of the visual system (Pollen and Ronner, 1983). Also these filters have been suggested to play a central role in human feature detection at early stages of the visual system (Morrone and Burr, 1988).

In physiological investigations, cells with different RF characteristics have been observed throughout the visual processing hierarchy. At the level of the retina, RFs typically display a concentric, center-surround, antagonistic structure. ON cells are excited by light at the center of the RF and inhibited by light at the surround – thus sensitive to light increments. OFF cells are excited by light in the surround of the RF and

[1] The collaborative research is supported by the German-Brazilian Academic Research Collaboration Program (DAAD-CAPES, Probral 1997, Project No. 70712). The research work by H.N. and T.H. is performed in the Collaborative Research Center on the "*Integration of symbolic and subsymbolic information processing in adaptive sensory-motor systems*" (SFB-527), which is located at the Univ. of Ulm and is funded by the German Science Foundation (DFG). L.P. is also supported in part by a CNPq/Brazil grant (520419/96-0).

[2] Authors' e-mail addresses: {hneumann,hansen}@neuro.informatik.uni-ulm.de, pessoa@cos.ufrj.br

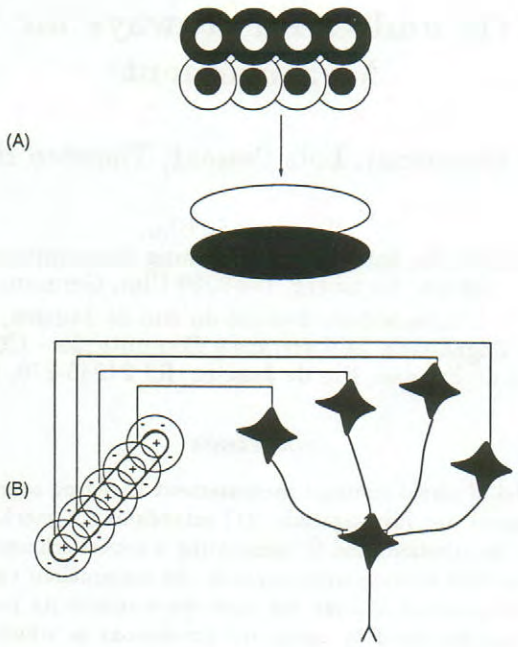

Figure 1: Cortical simple cell receptive fields (RFs). Hubel and Wiesel hypothesized that LGN cells with concentric, center-surround RFs project to the cortex with the proper arrangement so as to generate elongated RFs from unoriented ones. The ON regions of LGN cells project to ON regions of cortical cells, the same occurring with OFF regions. (A) Schematic representation of the combination of LGN signals. (B) Diagram highlighting the connections to cortical simple cells. Flashing a bar with an orientation that stimulates more of the excitatory centers (+) will stimulate the cell. Changing the orientation so that more of the inhibitory (−) surrounds are stimulated will diminish the cell's response.

inhibited by light at the center – thus sensitive to light decrements. Concentric ON and OFF cells are also found at the lateral geniculate nucleus (LGN) of the thalamus. It has been shown that ON and OFF cells actually comprise two independent parallel systems capable of signaling light increments and decrements (Schiller, 1992). At the level of the striate cortex, ON and OFF cells converge onto the same target cells (Fig. 1(A)). The classical work of Hubel and Wiesel (1962) revealed that cortical simple cells possess an elongated RF composed of a series of polarity-sensitive sub-fields.

How do cortical simple cells acquire their polarity-sensitive elongated RFs? Some transformation must be capable of generating the new cellular properties from the inputs received. Hubel and Wiesel (1962) hypothesized that a simple cell sub-field is generated directly by excitatory synaptic inputs from a row of LGN neurons whose RF centers overlap the sub-field. The ON sub-field would be generated from ON-center LGN cells, and the OFF sub-field by OFF-center LGN cells. As Fig. 1(B) illustrates, it is the proper alignment of the RFs of the projection LGN cells that generates the elongated cortical RF, thereby enabling cells to be sensitive to oriented contrast. The precise mechanisms responsible for orientation selectivity remain, however, a subject of intense investigation (see a recent review by Vidyasagar *et al.*, 1996). Nevertheless, there is evidence that an initial selectivity is brought about by the thalamo-cortical input arrangement (e.g., Ferster, 1988), in line with the original Hubel and Wiesel proposal.

Local contrast information near localized luminance transitions (or boundaries) not only signals the presence of a discontinuity but also carry information about the *surface qualities* of neighboring image regions. In lightness computation of flat scenes, such as in the Retinex theory (Land and McCann, 1971), by measuring the ratio of luminances at either side of a step transition, information about surface reflectance may be recovered. Such class of lightness algorithms first differentiates the image and subsequently threshold the result in order to maintain only contrast responses coinciding with sharp edge-like transitions. Shallow luminance gradients are thus "discounted." The edge information left after threshold suppression is then integrated in order to generate a lightness representation (Horn, 1974; Blake, 1985; Arend and Goldstein, 1987).

In all, in order to generate a reliable lightness estimate integration algorithms, such as Retinex, depend on a careful choice of threshold. A fixed threshold, however, cannot be determined for general scenes. This is because such algorithms need to register low contrast step-like transitions and remove shallow gradients at the same time. Thus if a low threshold is chosen, shallow gradients may be registered; if a high threshold is chosen, small contrast step-like transitions will be missed. This is a problem for the edge detection mechanisms mentioned above as their response amplitude is scaled with the local magnitude of the luminance gradient.

What is needed is a mechanism that is selective to the *shape* of the luminance transition – *i.e.*, whether they are abrupt or shallow. In this paper we develop a contrast detection circuit that exhibits such selectivity building upon a previous simplified implementation (Neumann and Pessoa, 1994). Our proposal makes use of the ON and OFF streams found in the visual system, which are independent at the levels of the retina and LGN and then merge at the level of the cortex, to determine whether abrupt or shallow luminance transitions are present. In a nutshell, the proposed circuit (1) produces strong responses whenever ON and OFF retinal responses occur next to each other, such as at a luminance edge[3]; while (2) producing non-zero responses when only ON or OFF retinal responses are present, such as due to shallow luminance gradients (e.g., luminance ramps, or a luminance sinusoid). As will be shown, circuit responses combine a linear as well as a non-linear "boosting" component.

In essence, two driving forces have shaped our investigation: (1) establishing a mechanism selective for sharp local transitions in the luminance distribution; and (2) generating a robust scheme of oriented contrast detection. Our starting point was the architecture of early stages in the mammalian visual system, as outlined above. Since the basic structure of the sensitivity profile of our proposed circuit closely resembles that of cortical cells selective for odd-symmetric contrast transitions, we refer to it as a *simple cell* circuit.

In the next section we will introduce the proposed circuit for contrast detection. For that purpose we first provide a formal description of the functionality of each model stage including a center-surround pre-processing stage and the elements of the non-linear circuit itself. We then investigate the circuit's capability of contrast detection providing an analysis of the steady-state response. We show that the circuit behaves as a *soft AND-gate* whose responses have two components: (1) a linear combination of ON and OFF channel contrast responses; and (2) a multiplicative, or gating-like, component whenever inputs to the ON and OFF sub-fields are spatially adjacent, or juxtaposed. The scale-space selectivity properties of the model are then analyzed in detail. Here we make use of the fact that the spatial sampling of the input sub-fields varies with the parametrization of the spatial input blurring of the initial contrast measures. We demonstrate that this amounts to a multi-scale scheme of Gaussian derivative operators beneficial to the non-linear input combination of adjacent contrast arrangements. Following this theoretical analysis we show results of computer simulations in which we selectively investigate key functionalities of the proposed contrast detection scheme. Finally, we relate the present model to other proposals that also have made use of non-linear or AND-gating processing for edge detection, most notably Marr and Hildreth (1980) and Iverson and Zucker (1995).

2 Neural Model for Oriented Contrast Measurement

Figure 2(A) shows the outline of the model. The input to the system is composed of two streams or channels, namely ON and OFF. The channels carry activations from initial processing stages having concentric center-surround RFs, as found at the retina and LGN. The model itself consists of a series of processing stages, each of which consists of a two-dimensional (2D) field (or grid) of processing units or cells. The input is also encoded as a 2D field of activity. All connections between model stages are topographically organized such that a spatial location (i, j) at a given stage connects to location (i, j) in the target field. The activation level at individual model stages represents the output value of the respective stages.

2.1 Model Stages

Center-surround interactions. The input luminance distribution, L, is processed by cells having center-surround, antagonistic, RFs, such as ganglion cells in mammalian retinae. The model includes both ON and OFF

[3] At an edge, ON responses will occur at the light side of the edge and OFF responses will occur at the dark side of the edge.

pathways that measure the degree of local luminance contrast in input images. Thus at every spatial location there are ON and OFF cells. These two fields of cells implement lateral inhibition that contrast-enhance, or sharpen, the input luminance distribution – cells respond strongly to (unoriented) luminance discontinuities.

A mechanism of local center-surround processing can be approximated by filtering the input distribution with difference-of-Gaussian filters[4] such as were originally proposed to model the receptive field structure of retinal ganglion cells (Rodieck, 1965; Enroth-Cugell and Robson, 1966):

$$net^+ = L \otimes \mathrm{G}_{\sigma_+} \quad \text{and} \quad net^- = L \otimes \mathrm{G}_{\sigma_-}, \tag{1}$$

where net^+ and net^- are net excitatory and inhibitory inputs for the ON center and OFF surround mechanisms in retinal Ganglion cells. The input luminance distribution is denoted by L, G_{σ_+} and G_{σ_-} are the respective Gaussian filters (parametrized by differently scaled space constants σ_+ and σ_-, respectively), and $\otimes$ implements the spatial convolution operator.

In classical proposals, such as e.g. in Rodieck (1965) or Marr and Hildreth (1980), the center and surround contributions combine linearly to determine the cell's response. As we already pointed out, the mechanism presented here has been developed in the context of joint processing of contrast as well as lightness and brightness information. The present approach therefore adopts a multiplicative, or shunting, formalism (Furman, 1965; Grossberg, 1970; Hodgkin, 1964), and thus follows a specification that takes into account visual *adaptation* processes that render responses sensitive to *luminance ratios*. Such formalization produces invariant responses for a given image regardless of overall illumination (and constant illumination gradients such as produced by a non-distant light source), such as exhibited by retinal ganglion cells. Essentially, contrast responses are obtained by dividing the signals of Equation 1 by the local average illumination.

Formally, for the ON channel, the activation y^+ generated is denoted by

$$\frac{d}{dt}y^+ = -\alpha_s y^+ + (\beta_s - \gamma_s y^+)net^+ - (\delta_s + \eta_s y^+)net^-, \tag{2}$$

where α_s, β_s, γ_s, δ_s and η_s are constants[5]; net^+ is the total excitatory input to y^+ and net^- is the total inhibitory input to y^+. These terms denote convolutions of the input L with Gaussian weighting functions, as indicated by Equation 1.

If we consider the equilibrium form of the above equation (i.e., $d/dt\, y^+ = 0$), with $\gamma_s = \eta_s = 1$ we obtain

$$y^+ = \frac{\beta_s net^+ - \delta_s net^-}{\alpha_s + net^+ + net^-}. \tag{3}$$

In other words, a linear combination of center (excitatory) and surround (inhibitory) mechanisms (numerator) is supplemented by a divisive term (denominator) that is sensitive to local average luminance. Therefore, for appropriate parameter ranges, cell responses are sensitive to input luminance ratios. OFF cell responses can be obtained by exchanging center and surround contributions above, such that we get

$$y^- = \frac{\beta_s net^- - \delta_s net^+}{\alpha_s + net^+ + net^-}. \tag{4}$$

A zero DC-level *linear* center-surround interaction is also covered by Equation 2 as a special case in which we set $\alpha_s = 1$, $\gamma_s = \eta_s = 0$ and $\beta_s = \delta_s$.

ON/OFF input to contrast cell sub-fields. The input to the circuit comprises ON and OFF contrast signals. RF elongation is obtained by sampling (via convolution) the activity distribution in the ON and OFF input channels with elongated (Gaussian) weighting functions. However, since we utilize a shunting mechanism for the initial center-surround processing stage, any possible residual non-zero DC level in activation has to be suppressed beforehand. It has been shown previously (see Neumann, 1993, 1996) that for any parameter setting $\beta_s > \delta_s$, the equibrium responses for y^+ and y^- contain a DC activity level $s^+ \propto (\beta_s - \delta_s)net^-$ and

[4] A difference-of-Gaussian filter assumes that both the center and surround components of retinal RFs can be modeled as Gaussian profiles of sensitivity. Larger spatial extents are obtained by employing Gaussians with larger standard deviation.

[5] Without loss of generality, we set $\gamma_s = \eta_s = 1$, which simplifies subsequent mathematical derivations for the shunting mechanism.

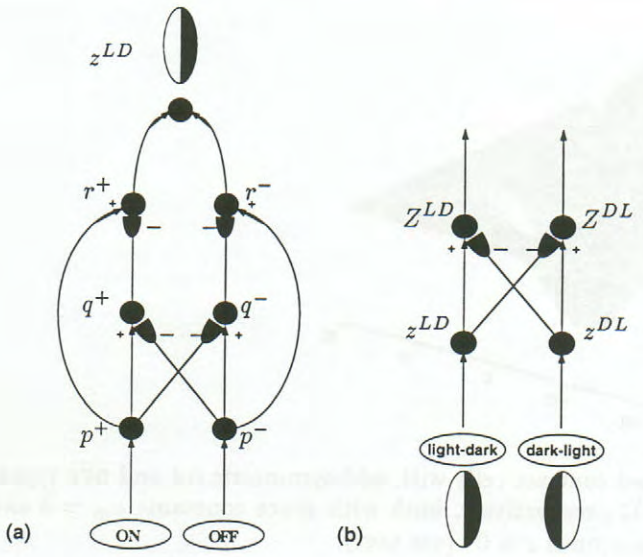

Figure 2: (a) Proposed circuit of contrast cell sensitive to light-dark contrast polarity. (b) Final competition of cells of opposite contrast polarity at each spatial location. Two types of forward interactions have been utilized. Those denoted with an arrow at the end in an excitatory fashion, those with an oval at the ending of a link are inhibitory.

$s^- \propto (\beta_s - \delta_s) net^+$, respectively. A stage of cross channel inhibition between y^+- and y^--activation guarantees for zero DC contrast activation at the input level for the simple cell circuit, independent of any parameter settings for β_s and δ_s. This inhibitory interaction to generate contrast activation is modeled by

$$\begin{aligned} c^+ &= \mathcal{R}[y^+ - y^-] \propto (\beta_s + \delta_s) \cdot \mathcal{R}[net^+ - net^-] \quad \text{and} \\ c^- &= \mathcal{R}[y^- - y^+] \propto (\beta_s + \delta_s) \cdot \mathcal{R}[net^- - net^+], \end{aligned} \tag{5}$$

with $\mathcal{R}[x]$ to denote a rectification operation that equals $\max[x, 0]$[6].

The spatial branches of contrast cells receive excitatory inputs from the ON and OFF contrast channel, depending on the arrangement of excitatory and inhibitory sub-fields. This input is sampled separately using elongated weighting functions with a smoothly decaying effective coupling strength. Before integration of contrast activity for excitatory and inhibitory sub-fields, the activities in both contrast channels undergo a local competition at each spatial location. It turns out that this competitive interaction also serves as a mechanism to generate a sufficient initial orientation tuning of the cell. In formal terms, the input to either sub-field of the circuit is modeled by

$$\begin{aligned} p^+ &= \mathcal{R}[(c^+ - c^-) \otimes \lambda_\varepsilon^+] \quad \text{and} \\ p^- &= \mathcal{R}[(c^- - c^+) \otimes \lambda_\varepsilon^-] \end{aligned} \tag{6}$$

(see Fig. 2), where the kernel λ determines an elongated spatial sampling function of orientation ε.

These inputs are used to detect local contrast changes of a given polarity, such as the presence of edges or other abrupt luminance variations. In our simulations we used elongated 2D Gaussian weighting functions for modeling the sensitivity profiles of $\lambda_\varepsilon^\pm$ (see Fig. 3), with space constants σ_m and σ_M to denote the minor and the elongation axis, respectively. In formal terms the anisotropic weighting kernel can be described by

$$\lambda_\varepsilon = N_\sigma \exp\left[-\frac{1}{2}\left(\vec{x}^T R_\varepsilon^T C_{mM} R_\varepsilon \vec{x}\right)\right], \tag{7}$$

where N_σ is a scaling constant, $\vec{x}^T = (x\, y)$ denotes the (transposed) vector of the spatial location, C_{mM} is the diagonal matrix

$$C_{mM} = \begin{pmatrix} 1/\sigma_m^2 & 0 \\ 0 & 1/\sigma_M^2 \end{pmatrix},$$

[6] It can be directly verified that this scheme also works for the special case in which the contrast channels already carry zero-DC level activities. If the input is generated by a linear center-surround interaction (as indicated above) the contrast channels carry activations $c^\pm = 2\beta_s \mathcal{R}[net^\pm - net^\mp]$.

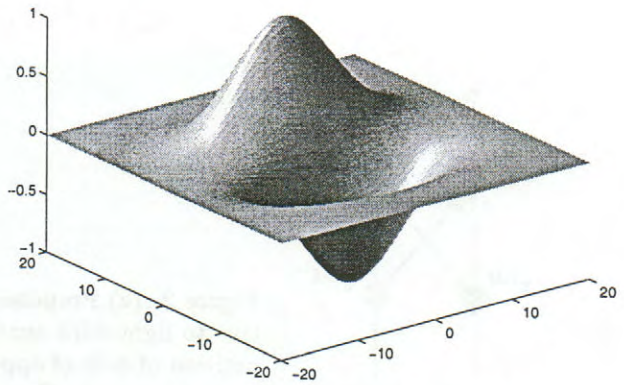

Figure 3: Effective spatial sensitivity profiles of oriented contrast cells with odd-symmetric ON and OFF input. The model uses elongated Gaussian profiles, λ_ε^+ and λ_ε^-, respectively, both with space constants $\sigma_m = 3$ and $\sigma_M = 2\sigma_m$; relative offset has been set to $\tau = 3$, orientation is $\varepsilon = 0°$ (see text).

determining the spreading along the principal axes, and R_ε determines the matrix of rotation in 2D (x, y)-space

$$R_\varepsilon = \begin{pmatrix} \cos\varepsilon & \sin\varepsilon \\ -\sin\varepsilon & \cos\varepsilon \end{pmatrix}.$$

The axis of elongation indicated by ε determines the preferred orientation of the cell.

In all cases we used balanced weighting functions for excitatory and inhibitory sub-fields, such that $\lambda_\varepsilon^+ = \lambda_\varepsilon^-$. By varying the space constants σ_m and σ_M of the elongated weighting functions one gets kernels of different spatial extent in length and width. This defines a family of kernels denoted as λ_ε^{S+} and λ_ε^{S-} where S denotes the spatial scale (see the notion of scale below in Section 3). The relative spatial offset $offset$ of these sub-fields (see Fig. 3) varies as a function of the space constant σ_m, such that we have $\tau(\sigma) = \sigma_m$.

Sub-field opponent interactions. The second stage of the circuit contains direct excitatory inputs from each ON or OFF sub-field (second term in equation below), as well as an opponent (inhibitory) interaction between channels (third term). The activity of the ON sub-field is given by

$$\frac{d}{dt}q^+ = -\alpha_c q^+ + p^+ - \beta_c q^+ p^- \tag{8}$$

where α_c and β_c are constants of this shunting inhibitory interaction. For the OFF sub-field we get

$$\frac{d}{dt}q^- = -\alpha_c q^- + p^- - \beta_c q^- p^+, \tag{9}$$

assuming the same setting of constants in both channels of the circuit.

Direct input and post-opponency signals combined. The third stage receives channel-specific inputs from both the first (excitatory; second term in equation below) and second (inhibitory; third term) stages. Formally,

$$\frac{d}{dt}r^+ = -\gamma_c r^+ + p^+ - \delta_c r^+ q^+ \tag{10}$$

where γ_c and δ_c are constants of this second stage of the circuit. OFF channel activations are obtained by exchanging '+' and '−' indices above. We get

$$\frac{d}{dt}r^- = -\gamma_c r^- + p^- - \delta_c r^- q^-, \tag{11}$$

again assuming here that the same setting of constants hold for both channels.

The functionality of the sub-circuits realizing each separate sub-field channel is to generate a self-inhibition, thus normalization, of the input activity distribution. The opponent interaction between these channels and the corresponding overall net activity will be discussed under functional aspects further below.

The final response for a light-dark cell is obtained by pooling ON and OFF activities. We formalize this as a simple linear combination by summing both r-activities. For this cell sensitive to light-dark (LD) transitions we get

$$z^{LD} = r^{+} + r^{-}. \tag{12}$$

The dark-light (DL) response, z^{DL}, is obtained in a corresponding manner, such that the respective ON and OFF input streams are flipped in their spatial arrangement.

Mutual inhibition of cells. Cells sensitive to opposite contrast polarity at the same spatial position finally undergo mutual inhibition, as indicated in Fig. 2(B). In functional terms, such a competitive stage helps to sharpen the activity profile generated by each cell sensitive to opposite contrast polarity alone.

The final cell responses are computed as

$$\begin{aligned} Z^{LD} &= \mathcal{R}[z^{LD} - z^{DL}] \quad \text{and} \\ Z^{DL} &= \mathcal{R}[z^{DL} - z^{LD}]. \end{aligned} \tag{13}$$

2.2 Relationship to Cortical Simple Cell Physiology

Several design issues as well as functional properties have strong relationships to findings about simple cell physiology. For example, we utilize oriented spatial weightings to model elongated sub-fields for integrating nonoriented input from cells with concentric RF outline (see Fig. 1). This is consistent with evidence that an initial selectivity is brought about by the thalamo-cortical input arrangement (e.g., Ferster, 1988), in line with the original Hubel and Wiesel proposal. Furthermore, we have utilized a local competition of contrast channels before integrating sub-field activities. This approach implements the opponent inhibition mechanism for simple cell sub-fields as described in Ferster (1989) (see also Tolhurst and Dean, 1990). Also, using partially overlapping spatially offset sub-field weighting functions has been suggested by the findings of Heggelund (1981, 1986) as well as Ferster (1988).

Our circuit integrates the activity from the corresponding sub-field (ON or OFF) in an excitatory fashion, while the opponent influences this by inhibitory action. This scheme now realizes a mechanism of opponent inhibition *between* sub-fields, similar to those in other simple cell models (see Pollen and Ronner, 1983). The mutual inhibition of cells with opposite polarity selectivity follows the description in Liu *et al.* (1992) who suggest the mutual inhibition between members of pairs of phase-related opposite contrast simple cells. Also Ferster (1988) provided evidence for a partial overlap of ON and OFF sub-fields in simple cells and suggested that competition between simple cells of opposite contrast polarity occurs at each spatial location.

In all, although we do not attempt to explicitly model the underlying mechanisms of cortical simple cells, with respect to orientation selectivity, spatial input sampling, etc., our model incorporates main principles of the structure and organization known from simple cell physiology. We therefore claim that our model circuit also serves as an abstract description of information transformation at early stages in the mammalian visual system.

2.3 Functionality of the Circuit

Equilibrium response. It is possible to gain insight into the precise functionality of the model, especially with regard to its AND-gate behavior, by assuming that cells reach equilibrium fast (i.e., $dx/dt = 0$) and lumping together the corresponding expressions. The activation r in the ON and OFF branches can thus be computed analytically. An assumed symmetry relationship between both channels can be achieved by setting the identity $\delta_c = \beta_c \gamma_c$. In this case, for a light-dark cell we get

$$r^{+} = \frac{p^{+}}{\alpha_c \gamma_c + \delta_c (p^{+} + p^{-})} \left(\alpha_c + \beta_c \, p^{-}\right) \quad \text{and}$$

$$r^- = \frac{p^-}{\alpha_c\gamma_c + \delta_c(p^+ + p^-)}\,(\alpha_c + \beta_c\, p^+)\,, \tag{14}$$

respectively. The final response for a contrast cell selective to light-dark polarity is computed as $z^{LD} = r^+ + r^-$. By using Equation 14 we get

$$z^{LD} = \frac{1}{\alpha_c\gamma_c + \delta_c(p^+ + p^-)}\,(\alpha_c\,(p^+ + p^-) + 2\beta_c\, p^+p^-)\,. \tag{15}$$

The response of a dark-light selective cell, z^{DL}, is obtained in a corresponding manner. In the final steady-state response, however, the roles of p^+ and p^- are interchanged.

This demonstrates the non-linear interaction of activity between the two branches. The basic functional properties of the model could be highlighted by the following more compact notation of Equation 15 that reads

$$z = \mathcal{L}\cdot(p^+ + p^-) + \mathcal{N}\cdot(p^+\cdot p^-)\,. \tag{16}$$

Here, $\mathcal{L}$ and $\mathcal{N}$ denote transformations of the initial contrast activities in the ON and OFF channel that generate the inputs to the circuit. In particular, we have $\mathcal{L} = \alpha_c\cdot\Gamma(c^+, c^-)$ and $\mathcal{N} = 2\beta_c\cdot\Gamma(c^+, c^-)$ with $\Gamma(c^+, c^-) = (\alpha_c\gamma_c + \delta_c(p^+ + p^-))^{-1}$. In $\Gamma(\cdot)$ the input activities $p^\pm$ for each individual lobe are themselves functions of c^+ and c^- (see Equation 6). Input to the model circuit is integrated linearly from both channels. Spatially adjacent activity (in the ON *and* OFF pathways) is signalled by an additional correlational (gating-type) component. The relative contribution of additive and gated activities is controlled by the (shunting) parameters α_c and β_c in Equation 8. Moreover, the activity self-normalizes with respect to the total input activity from the ON and OFF channel (function $\Gamma(c^+, c^-)$ above). The model thus relates to the scheme proposed by Carandini and Heeger (1994) in which activity of cortical neurons is normalized through division of pooled activity from a large number of cells.

Linear and non-linear responses. In all, the model behaves as a *soft AND-gate* that boosts adjacent ON and OFF signal configurations but that also responds to other configurations – albeit in a reduced manner. In terms of the circuit shown in Fig. 2(A), it is the opponent inhibition of the second stage (signals q^+ and q^-) associated with the within-channel inhibition (from the second to the third stage) that implements the soft AND-gate behavior. These interactions produce a mechanism for *disinhibition* that generates large outputs only when *both* ON and OFF channel inputs are large. To understand this consider the case where, say, only ON signals are input to the model; the OFF pathways are thus shut down. Responses will be small since the (within channel) inhibition from the second to the third stage will attenuate the input signal via a normalization mechanism. Now consider the case when there are potent inputs to both ON *and* OFF channels. The cross inhibition between the first and second stages will largely reduce second stage activities (signals q^+ and q^-). These by their turn will not be able to inhibit stage three signals and the original inputs will be able to combine at the last stage (z^{LD} and z^{DL}) since they reach it via the "side pathways" from the first to third stage. We see that the presence of inputs in both channels leads to a disinhibition in the circuit and hence powerful responses. In all, the circuit detects when there are adjacent ON and OFF signals, hence generating the soft AND-gate behavior.

The relative proportion of linear and non-linear response is controlled by the parameters α_c and β_c. The net input scaling by the saturation levels of initial ON- and OFF-channel processing also directly contributes to the contrast cell response in a systematic fashion. Equations 5 and 6 demonstrate that the ON and OFF channel input to oriented sub-fields is denoted by

$$p^\pm \propto (\beta_s + \delta_s)\cdot\mathcal{R}[(net^\pm - net^\mp)\otimes\lambda^\pm_{\vec{c}}]. \tag{17}$$

We observe for a given net input that the relative proportion of the non-linear contribution in Equation 15 is $\beta' = (\beta_s + \delta_s)\cdot\beta_c$. For any further analysis one must therefore take into account the range of activities generated in the initial center-surround preprocessing stage. For convenience, an activity range of [0..1] from initial center-surround filtering has been ensured in all our simulations.

The key idea behind our model is that contrast changes are better localized by a circuit that is selectively sensitive to abrupt luminance transitions. These transitions will be invariably associated with adjacent ON and OFF contrast signals (for some spatial scale; see below). A linear combination scheme is, of course, sensitive to such transitions, but not sensitive *enough* such that it shows only differential variations in response once previously adjacent activities in the ON and OFF channel will be shifted farther apart (see also du Buf, 1994).

3 Families of Receptive Fields and Selectivity to Spatial Scale

3.1 Elementary Properties

Motivation. The visual system is faced with the problem to measure relevant structure of the outside world. Real-world objects only exist as meaningful entities over certain ranges of measurement scales. An example stressed by Marr and Hildreth (1980) is the appearance of the fine textured veins of a leaf on a small scale but the overall shape and luminance variation appearing on a much coarser scale. Furthermore, more gradual intensity variations often relate to illumination variation or changes in surface orientation, whereas abrupt changes in the luminance distribution are often caused by transitions in surface properties, such as reflectivity (Horn, 1974). A vision system in general has no advance knowledge about the appropriate scales for analysis. Therefore, in order to deal with such a multitude of properties of real-world objects, the machinery of a vision system has to process the input luminance distribution at different scales (see e.g. Witkin, 1983; Koenderink, 1984; Lindeberg and ter Haar Romeny, 1994; and for a short tutorial, Lindeberg, 1996).

The raw luminance distribution is processed by an initial center-surround mechanism. After opponent-inhibition this activity is integrated by oriented offset weighting functions which define the excitatory and inhibitory sub-fields to an oriented cell. The signals for ON and OFF contrast response are rectified such that the contrast channels carry a single positively bounded data representation from the initial filtering stage. By utilizing weighting functions of different sizes, λ_ε^{S+} and λ_ε^{S-}, these contrast activities are blurred and sampled at increased relative spatial offsets, thus a family of cells sensitive to different spatial scales is introduced. The spatial scale attribute S itself is a function of the space constant σ, thus $S = S(\sigma)$ (see Equation 7).

Generation of scale-space derivative kernels. A contrast edge is processed by an initial center-surround filtering stage. The results are half-wave rectified and segregated into two separate representations for ON and OFF contrast, respectively. The results of individual ON and OFF response are blurred by oriented spatially scaled weighting functions to generate the input for the opponent contrast cell sub-fields of different sizes. This non-linear processing cascade is shown to be identical to a 1st order derivative kernel applied to the activation generated by the center-surround processing.

To simplify the mathematical analysis we approximate the initial center-surround filtering by a Laplacian-of-Gaussian (LoG) operator. The response of such filter processing a step input function, modeled as a Heaviside function $\mathcal{H}$, results in a profile of a 1st order derivative of a Gaussian, $D1\mathrm{G}$. This profile is an odd-symmetric function with positive and negative lobes. For a representation to carry positive signal responses only, the positive and negative lobes are half-wave rectified. We get

$$\begin{aligned} c^+(u) &= \mathcal{R}[\mathrm{LoG}_{\sigma_1}(u) \otimes \mathcal{H}(u)] = \mathcal{R}[\frac{d}{du}\mathrm{G}_{\sigma_1}(u)] \qquad \text{and} \\ c^-(u) &= \mathcal{R}[-\mathrm{LoG}_{\sigma_1}(u) \otimes \mathcal{H}(u)] = \mathcal{R}[-\frac{d}{du}\mathrm{G}_{\sigma_1}(u)], \end{aligned}$$

with $\mathcal{R}[x] = \max[x, 0]$. These responses are subsequently filtered by a Gaussian blurring function whose results are then combined to generate the edge response of the circuit. We get $s(u) = \mathcal{R}[\frac{d}{du}\mathrm{G}_{\sigma_1}(u)] \otimes \mathrm{G}_{\sigma_2}(u) + \mathcal{R}[-\frac{d}{du}\mathrm{G}_{\sigma_1}(u)] \otimes \mathrm{G}_{\sigma_2}(u)$. Since $\mathcal{R}[\frac{d}{du}\mathrm{G}_{\sigma_1}(u)] = \frac{d}{du}\mathrm{G}_{\sigma_1}(u) \cdot [1 - \mathcal{H}(u)]$ and $\mathcal{R}[-\frac{d}{du}\mathrm{G}_{\sigma_1}(u)] = -\frac{d}{du}\mathrm{G}_{\sigma_1}(u) \cdot \mathcal{H}(u)$ we can rewrite the final response to get

$$s(u) = \frac{d}{du}\mathrm{G}_{\sigma_1}(u) \otimes \mathrm{G}_{\sigma_2}(u) = \frac{d}{du}\mathrm{G}_{\sqrt{\sigma_1^2+\sigma_2^2}}(u). \tag{18}$$

This demonstrates the equivalence of our hierarchical processing scheme based on segregated representations of ON and OFF activations and an approach that utilizes filters derived from an analytic description of 1st order derivative operations. It also verifies that the subsequent blurring of separated contrast channel responses of one frequency band – generated by the initial center-surround processing stage – produces results equivalent to those achieved with a bank of scaled center-surround filters.

Opponent offset blurring approximates 1st order derivative filtering. The kernels $\lambda^\pm$ were spatially offset slightly by an amount τ relative to the reference location of the target cell. They collect responses

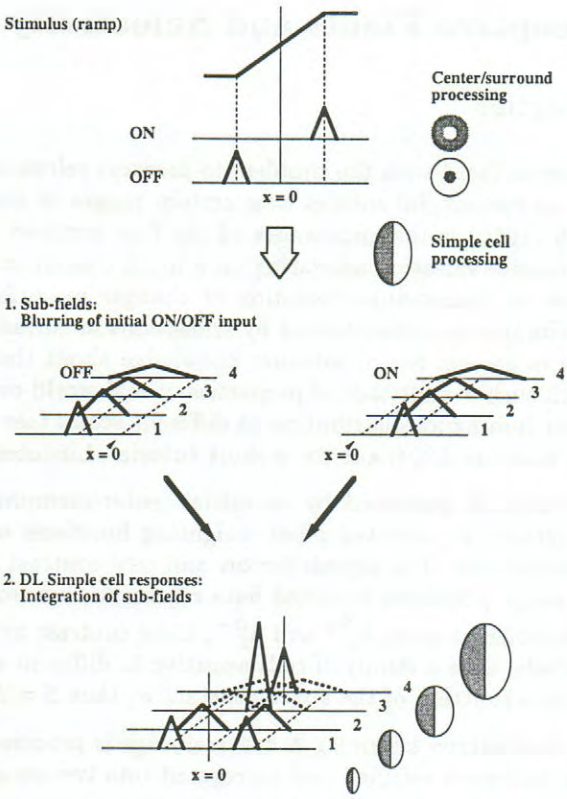

Figure 4: Responses of a scaled family of contrast cells sensitive to an odd-symmetric dark-light (DL) luminance transition (ramp contrast). Top: Input stimulus is shown together with schematic ON and OFF responses generated by the initial stage of center-surround processing. These responses of either contrast channel appear at the "knee points" of the plateaus. Depending on the width of the ramp relative to the size of the initial center-surround filter they appear in spatial isolation (as shown in the sketch) or juxtaposed. Middle: Increased blurring of initially isolated contrast responses for a wide transition ramp. Four different scale selectivities are shown with reference to the location at the center of the ramp ($x = 0$). These blurred activations provide the inputs to cells sensitive to DL transitions. Bottom: Responses of contrast cells for the four scales that integrate their input to sub-fields from increasingly distant offsets (the display of responses for light-dark (LD) cells has been omitted in order to keep the sketch simple). For a cell at a more coarser scale ON and OFF inputs appear to be juxtaposed such that the non-linear component can contribute via its ignition. As a consequence, a unique maximum response is generated as a function of scale.

in the ON and OFF contrast channels to be further processed in the circuit. The difference of spatial offset Gaussians closely resembles the profile of a 1st order derivative operation. To show this, consider the model of a parametrized ramp edge transition in a local (u, v)-gauge coordinate system where the u-axis is oriented along the contrast profile. Assuming an intrinsically 1D luminance variation we can treat the response of an optimally tuned operator for contrast detection in a single dimension. The 1st order derivative of a Gaussian ($D1G$) is given by $d/du\, G_\sigma(u)$. We define a finite unit-area impulse function as the difference of two slightly offset Heaviside functions

$$\Pi_{R=2\tau}(u) = \frac{1}{R}\left[\mathcal{H}(u+\frac{R}{2}) - \mathcal{H}(u-\frac{R}{2})\right], \quad \text{with} \quad \mathcal{H}(u) = \begin{cases} 0 & \text{if } u < 0 \\ 1 & \text{if } u \geq 0 \end{cases}$$

(see Bracewell, 1978). Convolution of the unit-area impulse with the $D1G$-function gives

$$\frac{d}{du}G_\sigma(u) \otimes \Pi_{R=2\tau}(u) = \frac{1}{2\tau}\left[G(u+\tau) - G(u-\tau)\right].$$

Utilizing a coordinate transform $u^* = u - \tau$, setting $\Delta = 2\tau$ and then taking the limit, $\Delta \to 0$, the finite impulse function Π degenerates into an infinite impulse or δ-function. The convolution of any function with δ

follows the Fourier sifting property such that we finally get

$$\lim_{\Delta \to 0} \left[\frac{d}{du} \mathrm{G}_\sigma(u^*) \otimes \Pi_\Delta(u^*) \right] = \frac{d}{du} \mathrm{G}_\sigma(u^*). \tag{19}$$

Thus, the difference of offset Gaussians with space constant σ thus approximates – up to a scaling – a $D1G$ with the same parameter setting.

Responses as a function of scale. We now consider the processing of a luminance transition with a ramp profile of a priori unknown width (compare du Buf, 1993, 1994). The suggested model is sensitive to the spatial adjacency of retinal ON and OFF signals. Spatial proximity however is a relative measure that will depend on the *spatial scale* of processing. What may be spatially proximal for a large scale may be distant for a small one. Sensitivity to spatial scale endows model cells to selectively process a given visual structure, such as the ramp transition shown in Fig. 4. For a wide transition ramp the initial center-surround processing generates isolated ON and OFF contrast responses which are located at the shoulders ("knees") of the ramp transition. A cell with a RF selective to odd symmetric contrast variations located at position $x = 0$ at the center of the ramp for the smallest scale receives no input from either blurred ON or OFF contrast channel (compare scale 1 in Fig. 4 *middle, bottom*). Cells slightly offset to either side of this central location receive input from only one sub-field (lobe) and thus generate normalized linear responses. As the blurring proceeds more diffuse distributions of ON and OFF contrast responses appear which eventually meet at the center of the ramp such that they appear to be juxtaposed for the coarse scale at location $x = 0$ (scales 3 and 4 in Fig. 4 *bottom*). Now integrated inputs from *both* sub-fields add and a superimposed component is generated by the *product* of the magnitude of these inputs. If the product is sufficiently high in amplitude the latter contribution facilitates the target cell activation by an additional "boost". The spatial juxtaposition of ON and OFF input activation to the circuit signals a transition which is sharply localized relative to the current spatial scale.

The circuit is thus selective for the input structure with sharp contrast transitions. The *quantitative* properties of the cell responses in scale-space can be derived from the steady-state activation given in Equation 15. Below we present the results of this investigation.

3.2 Quantitative Analysis of Scale-Space Response

In this subsection we summarize the *quantitative* findings for responses generated by scaled contrast cells which are applied to different idealized luminance transitions. We first show the results derived for step edge responses. This motivates the subsequent derivation for the results processing the gradual transition of a ramp as discussed above. In both studies we compare the results for the non-linear circuit with those generated by a scheme of linear filtering. Detailed results of investigations can be found in Appendices 1 and 2.

We utilize the compact notation of non-linear response of the circuit that is given by

$$z = \mathcal{L} \cdot \left((p^+ + p^-) + \frac{\mathcal{N}}{\mathcal{L}} \cdot (p^+ \cdot p^-) \right) \tag{20}$$

(compare with Equation 16). For the quantitative analysis we omit the gain $\mathcal{L}$ and only consider the expression given in brackets. For the gain of the non-linear component we define

$$\mathcal{N}' \equiv \frac{\mathcal{N}}{\mathcal{L}} (\beta_s + \delta_s) = 2 \frac{\beta_c}{\alpha_c} (\beta_s + \delta_s) \tag{21}$$

(see Appendix 2). Based on these definitions we relate the linear and non-linear response components.

Step edge response. A step edge profile of height h is defined by a Heaviside function,

$$f_{step}(u) = h \cdot \mathcal{H}(u), \tag{22}$$

in which the u-axis is taken in the direction orthogonal to the local orientation tangent to the luminance contrast. Processing this input first by a center-surround filter (approximated by a Laplacian-of-Gaussian) subsequently followed by a 1st order (Gaussian) derivative filtering generates a response profile with a unique

maximum at the step location $u = 0$. For the non-linear circuit the segregated contrast responses always appear to be juxtaposed at either side of the contrast step. The relevant component of response (contribution given in brackets in Equation 20) of the non-linear circuit at the location of the luminance step is given by

$$s_{\text{step}}{}^{nl}(u=0) = \frac{h}{\sqrt{2\pi}\sigma^3}\left(1 + \mathcal{N}'\frac{1}{\sqrt{2\pi e}\sigma}\right). \tag{23}$$

This shows that for a linear as well as a non-linear cell the response is maximal for the smallest scale, i.e. it smoothly drops down as blurring increases. Furthermore, it shows that the non-linear contribution only gets significant for a gain $\mathcal{N}' \gg \sqrt{2\pi e}\sigma \approx 7\sigma$. Considering the definition of the gain in Equation 21 it is reasonable to treat the parameter β_c as a non-zero function of σ.

Ramp edge response. A ramp edge profile of height h and width R is defined by

$$f_{ramp}(u) = h \cdot \mathcal{H}(u) \otimes \Pi_R(u). \tag{24}$$

In the limit, as $R \to 0$, the ramp converges to a step function as defined above. Again, we utilize the sequence of processing steps of center-surround filtering and 1st order Gaussian derivative operation. The latter is approximated by the individual blurring of the contrast responses followed by a numerical differentiation for final sampling the inputs from the sub-fields of the contrast cell. Now, depending on the ratio between the operator scale and the width of the ramp, σ/R, the ON and OFF contrast responses appear in isolation ($\sigma \ll R$) or juxtaposed similar to the case of a step transition ($\sigma \approx R$). For the position $u = 0$ at the center of the ramp we can now treat the response as a function of scale. For the *linear* model a relative maximum in response occurs at

$$\sigma_{max} = \frac{R}{2\sqrt{3}}. \tag{25}$$

For the analysis of scale-space response for the non-linear circuit, we investigate the additional contribution from (blurred) ON and OFF contrast responses sampled from offsets relative to the ramp center. The relevant component (bracket part in Equation 20) of the corresponding response for the circuit is

$$s_{\text{ramp}}{}^{nl}(u=0)|_{\sigma=\sigma_{max}} = \frac{48\sqrt{3}h}{\sqrt{2\pi}} \exp\left[-\frac{3}{2}\right] \cdot \frac{1}{R^3} \cdot \left(1 + \mathcal{N}'\frac{\sqrt{2}}{8\sqrt{3\pi}}\frac{h}{R}\exp\left[\frac{3}{2}\right]\right). \tag{26}$$

This shows that there exists an optimum scale for processing a ramp edge of a priori unknown width and height. The non-linear contribution is itself dependent from the slope of the ramp and gets significant for a gain $\mathcal{N}' \gg 4\sqrt{6\pi}\exp\left[-\frac{3}{2}\right] m^{-1} \approx 4m^{-1}$, where $m = h/R$

The non-linear circuit shows a multitude of desired principles. For one, the additional "boosting" of activity helps to drive the cell output to generate a response that is maximal in absolute terms. It is shown in Appendix 2 that the non-linear cell tuned to an optimum scale generates *absolute* maximum amplitude responses. In addition, the contribution generated by the non-linearity depends on the scale σ (step) or on the slope m (ramp) of the luminance transition. The parameter to control the efficacy of the non-linear contribution in $\mathcal{N}'$ is β_c, the gain of opponent shunting inhibition in the circuit (see Equations 9 and 8). The gating of contrast activations – adding to the (linear) cell response – enables the circuit to preferentially respond to sharp transitions, irrespective of their height. This selective functional property was one of the principal motivations for the development of the circuit in the context of the modeling of functional mechanisms for neural contrast and brightness processing (Neumann and Pessoa, 1994; Pessoa *et al.*, 1995).

4 Simulations

In this section we evaluate the model on the basis of a series of computer simulations that demonstrate the functionality. The section is organized as to start with the demonstration of the usefulness of the approach for image processing purposes. We tested its robustness to noise in comparison with a corresponding pure linear model and demonstrated its selectivity in automatic scale selection, all based on synthetic test images. The computational relevance is also demonstrated by means of natural images from a test data set. Since we

have also shown that the model accounts for some relevant properties of cortical simple cells that are usually believed to behave almost *linearly*, we conducted an experiment showing that our *non-linear* circuit also shows substantial linear behavior. We then finally show results that demonstrate the usefulness of the model as a first step in a processing hierarchy in which initial measurements are grouped together in order to generate meaningful chunks for shape recognition. In particular, we show the model's strength in the initial measurement for subsequent integration by long-range grouping processes.

In all simulations, responses are shown after mutual inhibition (Z^{LD} and Z^{DL}). Luminance values of input images have been normalized to the range of [0..1]. The initial center-surround processing stage involves shunting interaction and subsequent haf-wave rectification to generate segregated ON and OFF channels (see Section 2.1). Model parameters for this initial stage were set to $\alpha_s = 0.5$, $\beta_s = 1.0$, and $\delta_s = 0.1$ (as already pointed out above, we set $\gamma_s = \eta_s = 1.0$ in order to yield symmetric normalization in both channels). Parameters of isotropic Gaussians were set to $\sigma_+ = 1.0$ and $\sigma_- = 3.0$, respectively, thus getting a $1:3$ center-surround ratio. The model parameters of the non-linear circuit were set to $\alpha_c = 1.0$, $\beta_c = 10000.0$, $\gamma_c = 0.01$, and $\delta_c = 100.0$. Their specific choice is non-critical as long as the linear components scaled by α_c and γ_c are small compared to the cross-channel inhibition effect. The Gaussian weighting functions were elongated by a $\sigma_M : \sigma_m = 2:1$ ratio; the variance σ_m is measured in pixels along the short axis. The separation τ grows linearly with the variance (scale S). Eight discrete, equally spaced orientations were processed. The corresponding linear circuit was approximated simply by eliminating the opponent interaction between the sub-fields in the non-linear contrast cell circuit (stages $q^{\pm}$ and $r^{\pm}$, see Fig. 2). Thus the scheme used for comparison directly integrates the activity from both sub-fields, namely $z = p^+ + p^-$.

4.1 Image Processing

As indicated we start to demonstrate the capacity of the circuit on the basis of synthetic as well as real camera images from a test set. Test simulations run on synthetic data were to justify the robustness of the model against noise and the selectivity of the mechanisms to scale. Results generated for natural images are intended to serve for comparison of performance with other known methods.

Synthetic images. A first strict test of an image processing algorithm consists in probing it with *noisy* images. Figure 5 shows a synthetic image containing an elliptic region embedded in a lighter background and a cross-section profile (left). The entire image was corrupted by Gaussian noise (half width 50% amplitude). Figure 5 (middle) shows the output of the new model revealing that it is capable of accurate contour localization even in the presence of non-trivial noise levels. It is also instructive to compare the performance of the circuit with the linear scheme. As shown in Fig. 5 (right), the linear scheme is less robust to noise as it also shows less selectivity in terms of edge localization. Note that no post-processing such as final thresholding operations were performed – these could be used to remove the low intensity spurious signals due to noise.

In order to evaluate the theoretical derivations on the mechanism's selectivity to spatial scale we have conducted a series of experiments based on the processing of scaled gradual luminance transitions, namely ramps. Figure 6 illustrates the spatial frequency selectivity of the non-linear model by comparing its behavior with the analogous linear scheme. For the non-linear contrast cell, as the spatial scale of operation is increased, cells whose centers are more closely to the middle of the ramp, eventually become ignited by the non-linear proportion of the response. That is, by using larger elongated Gaussian operators that sample the blurred ON and OFF sub-field input target cells conjointly receive input from offset positions as they appear to be juxtaposed in a coarser scale – a maximum response is produced at the middle of the ramp. This behavior should be contrasted to that of the linear scheme. It can be recognized that although maxima evolve at the middle of the ramp they are only *local* such that *absolute* maximum response appear at a fine spatial scale, localized to the left and right of the knee points.

Natural images. Natural images provide a good test of the image processing capabilities of our model of contrast detection. In particular, we can assess the contrast localization properties of the model by again comparing its output with that produced by an analogous linear scheme. Figure 7 illustrates the better contrast localization properties of our circuit when compared to the linear scheme. We see that much sharper "edge signals" are generated by the circuit effectively registering the contour outlines present in the image.

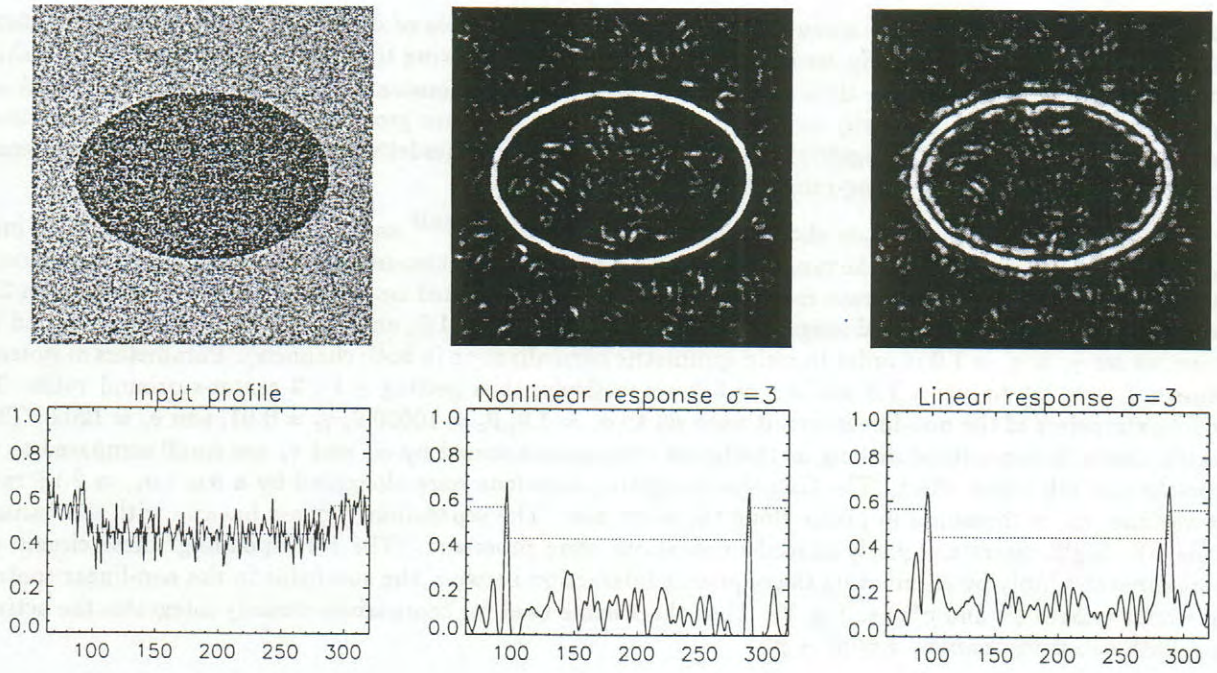

Figure 5: Synthetic image with noise. Input luminance distribution corrupted by additive Gaussian noise with 50% amplitude of contrast height (top left); pooled activity for all orientation fields generated by the non-linear circuit (top middle) and the linear circuit (top right). Corresponding 1D cross-sections of the above shown 2D distributions (bottom row).

4.2 Linear vs. Non-Linear Processing Behavior

We have pointed out above (see Subsection 2.2) that our model inherits a number of simple cell properties. We developed a *non-linear* circuit that pronounces any input configuration of juxtaposed ON and OFF activation thus being specifically selective to sharp luminance transitions. In order to justify the relevance of the model, it has to be demonstrated that the overall behavior does not in general contradict previous findings in physiology that have been taken as support for *linear* mechanisms driving simple cells. Candidate tests include the linear summing principle given increasing stimulus length and using Eigenfunctions of linear systems such as spatial sine-wave luminance modulations. Sine-wave stimuli have been used to characterize linear systems such as a linear filtering operation. In order to demonstrate the validity of our model to that respect we process a spatial cosine luminance waveform which result is shown in Fig. 8. It can be seen that the result generates a spatial distribution of activity that corresponds to the initial cosine modulation and is consistent with that predicted for a simple cell.

This demonstration shows that our circuit, although it is intrinsically non-linear, shows significant linear behavior especially demonstrated for test cases similar to experimental studies with sinusoidal luminance modulations.

4.3 Initial Measurement and Grouping

Glass patterns (Glass, 1969) illustrate how the visual system is capable of employing local information to generate global structure. The perception of structure generated by a Glass pattern (or a variation of it) is based on two types of interaction: a local operation of feature measurement or token extraction and a long-range integration of local items (Sagi *et al.*, 1993).

A test of the initial mechanisms underlying Glass pattern perception was provided by a recent investigation

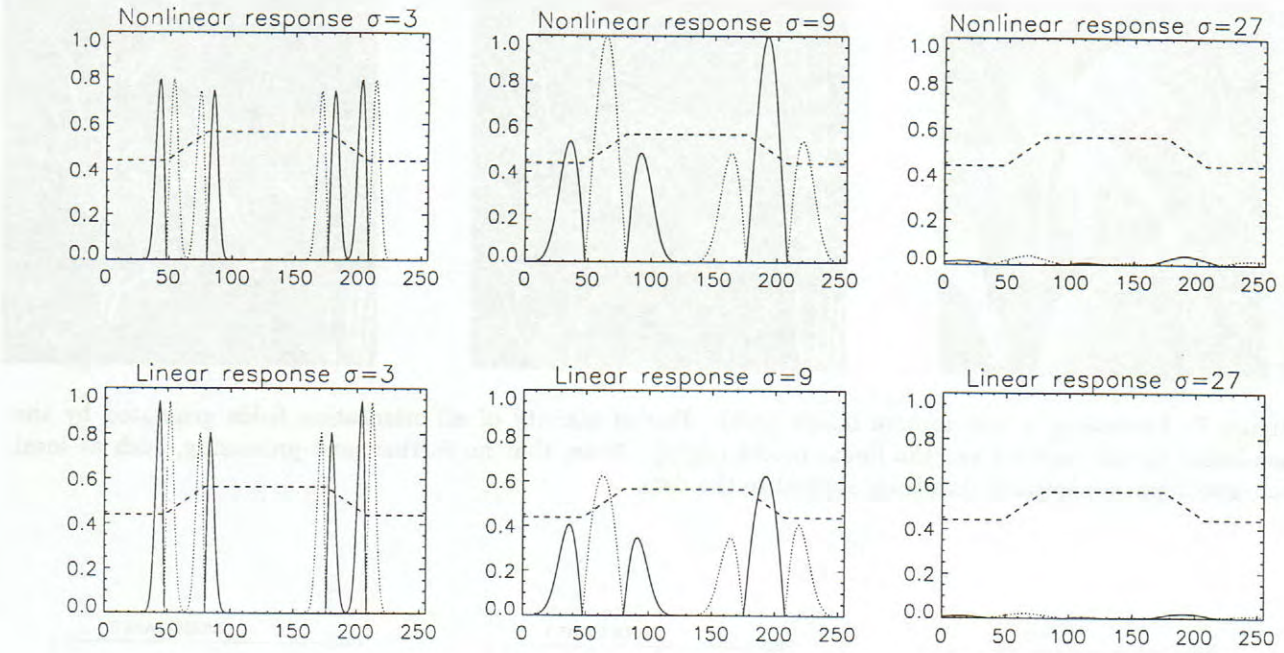

Figure 6: Scale-space selectivity. A ramp luminance distribution is processed at small, medium and large spatial scales. For better visualization of the responses, we plot a 1D cross-sections of the ramp as well as of responses generated with the non-linear circuit (top) and linear scheme (bottom). Responses are shown for light-dark cells (solid) and dark-light cells (dotted). The ramp widths were parametrized by $R = 32$ units.

by Brookes and Stevens (1991). In their study they generated Glass patterns using oriented white dot pair items which are either radially or circularly oriented. Due to the contrast sensitivity of oriented cells, the authors hypothesized that in a display the inclusion of an opposite polarity dark dot between the two white dots of each local pair ("dot-between" arrangement), should disrupt the perception of the structure seen without the distractor. In particular, the experiment was designed such that the disruption of a *radial* organization caused the pattern to be more likely perceived as circular. On the other hand, adding a black dot to disrupt a *circular* organization made by white dot pair items increases the tendency to perceive a radial organization. As a control, the "dot-between" case was varied so that the disrupting black dot was placed aside one of the white dots ("dot-adjacent" case). We show in Fig. 9 the input stimuli used for the radial test case. In Fig. 10 we show the local elements used as items for the generation of the different variants of Glass patterns. Brookes and Stevens (1991) reasoning was that if the perception of structure intimately depends on localized mechanisms sensitive to local contrast direction, perceived structure should be lost since the local oriented "dot-between" arrangement largely disrupts responses for the orientation of the white dot pair item. Even more, in the "dot-between" case a strong response in the orientation orthogonal to the item is predicted while the "dot-adjacent" case should have no disturbing effect (it may be even more supportive). The perceptual results confirmed this prediction. In an alternative-forced-choice judgement, there was a significant increase in the subjects' responses to orthogonal apparent organization (reversing concentric and radial) when the black dot was placed in the middle between the white dot pairs. The placement of the black dot adjacent to a white dot had no influence on the correct judgement of perceptual organization.

The experimental setting described above demonstrates that even tiny differences in the local arrangement of structure can cause categorical differences in the pattern perceived as a whole. We find this suggestive for a mechanism that is selective to even very small localized contrast patterns. Motivated by this observation we stimulated our circuit with the local dot arrangements shown in Fig. 10 and compared the results with those generated by a linear model. Each pattern was pre-processed by the initial stage of center-surround interaction, segregating representations of ON and OFF contrast. Figure 11 displays the results for all items used: white dot pair, white dot pair with black dot added in the middle ("dot-between"), and white dot pair with black dot

Figure 7: Processing a real camera image (left). Pooled activity of all orientation fields generated by the non-linear circuit (center) vs. the linear model (right). Note, that no further post-processing, such as local non-maximum suppression, has been applied to the data.

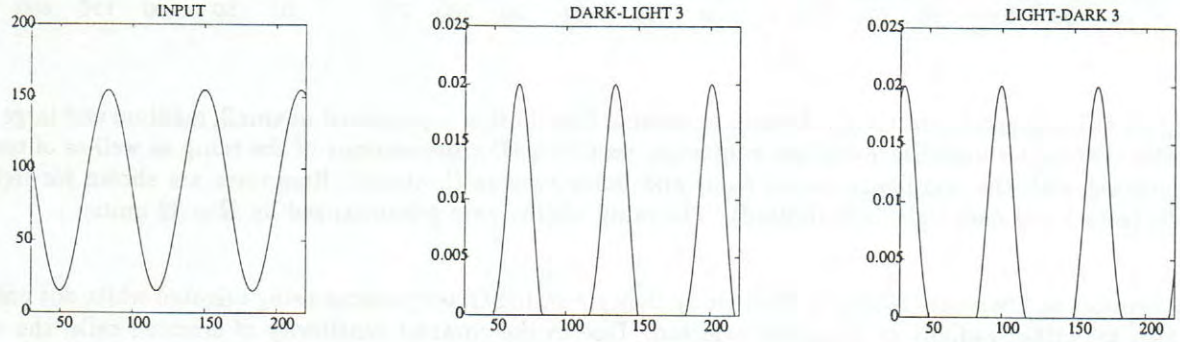

Figure 8: Processing results of the non-linear circuit generated for a 1D spatial luminance sine wave. The input signal is shown on the left, the responses for two simple cells sensitive to opposite contrast (dark-light (DL), light-dark (LD)) are shown in the middle and in the right panel, respectively. As predicted for a pure *linear* cell symmetric responses occur for opposite contrast sensitivities at the positive and negative slopes of the sine wave.

added aside ("dot-adjacent"). For each of these inputs we show the results for non-linear and linear processing. In order to gain more insight into the orientation specificity of the generated activations, we produced "needle" diagrams to encode individual response magnitudes for the different orientations. The certainty of orientation selectivity serves as an indicator for clarity of subsequent long-range integration mechanisms for grouping (Sagi *et al.* (1993); see computational mechanisms by, e.g., Grossberg and Mingolla (1985)). We show the results generated by the non-linear mechanism in the top row and the corresponding linear responses in the bottom row. For the white dot pair item (Fig. 11, left) the non-linear response shows a clear dominance along the orientation of the dot pair. The linear model also shows a certain preference in that direction but the response is much more blurred and the orientations are much more uncertain. For the "dot-between" stimulus (middle) the non-linear circuit generates a categorically different dominance which indicates a strong orthogonal contrast orientation. This coincides with the observation in psychophysical experiments that the correct organization is disrupted and a perception of the orthogonal orientation appears. In the "dot-adjacent" case (right) the correct organization is not disturbed as the overall dominance of orientation in the response is similar to the white dot pair. Between the pair of white and black dots, contrast responses of high amplitude are generated which support the overall orientation preference. In comparison to the result of the white dot pair alone the spatial distribution of responses appears more blurred. We suggest that the increased blurring weakens the response in

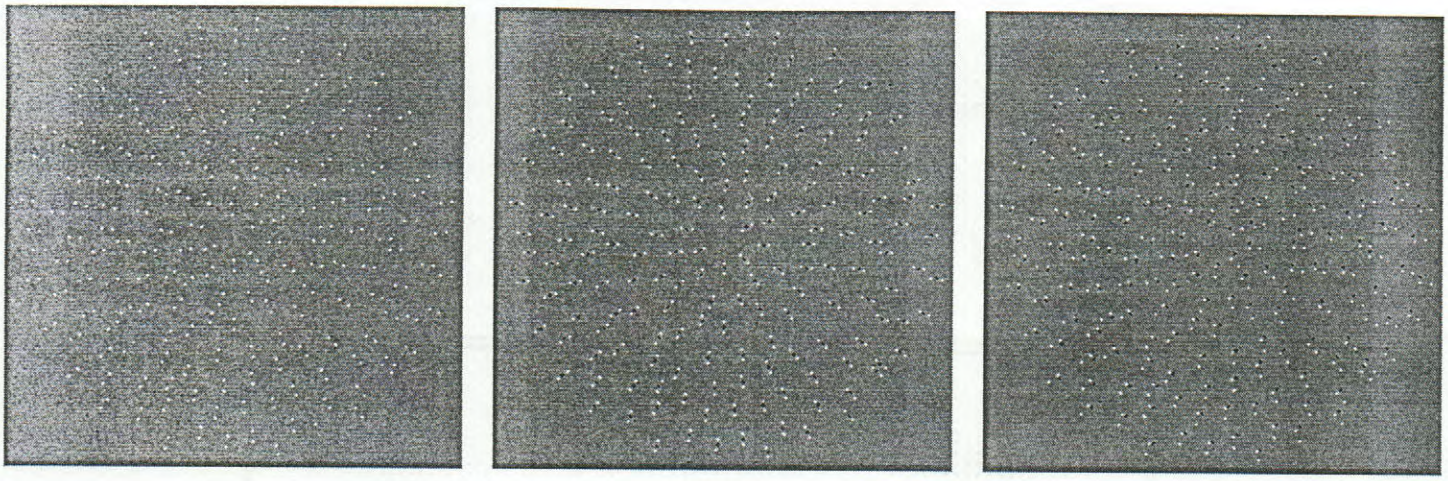

Figure 9: Displays of the different variants of Glass patterns from the radial test case used in the experiments of Brookes and Stevens (1991). Patterns with white dot-pair items, "dot-between" and "dot-adjacent" are shown from left to right. Each item in the radially oriented patterns is composed by local pairs of equal polarity and local triples of mixed polarity dots (see figure below). Please note, that due to reduced resolution and additional discretization the perceptual effect may be significantly reduced. However, in our original displays and the plates shown by Brookes and Stevens (1991) the variations produce significant effects.

the subsequent stage of integration for grouping and perceptual organization. The responses generated by the linear model also show preferences corresponding to those of the non-linear circuit although much weaker. In addition, as in the dot pair item the distribution appears much more blurred and more uncertain in orientation space. This would be insufficient for the grouping stage to switch between perceptually dominant orientations.

5 Discussion and Summary

We have introduced a circuit for non-linear contrast detection. The development was motivated by an analysis of the process of local structure measurement within luminance distributions. The proposed mechanism incorporates the local detection of contrast by measuring the amplitude of luminance changes, while at the same time accounting for the sharpness of any such change. The importance of the latter functionality was motivated by our earlier investigations in brightness perception (Pessoa *et al.*, 1995). However, as discussed in the introduction, such functionality is also important for robust contrast estimation in Retinex-like algorithms,

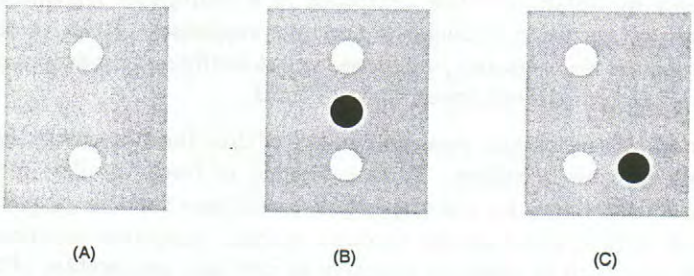

Figure 10: Sketch of local dot arrangements used in the Brookes and Stevens (1991) experiments to demonstrate categorical changes in the appearance of perceptual grouping in Glass patterns. (A) A local pair of white dots is shown as it appears in the original version of a Glass pattern. For the variation of this reference now a third dot of opposite polarity (black) is included. The dot was either placed (B) in the middle between the two ("dot-between"), such that it will break the collinear arrangement, or (C) aside one of the same polarity dots ("dot-adjacent"), such that the collinearity is supported by an aligned local contrast component.

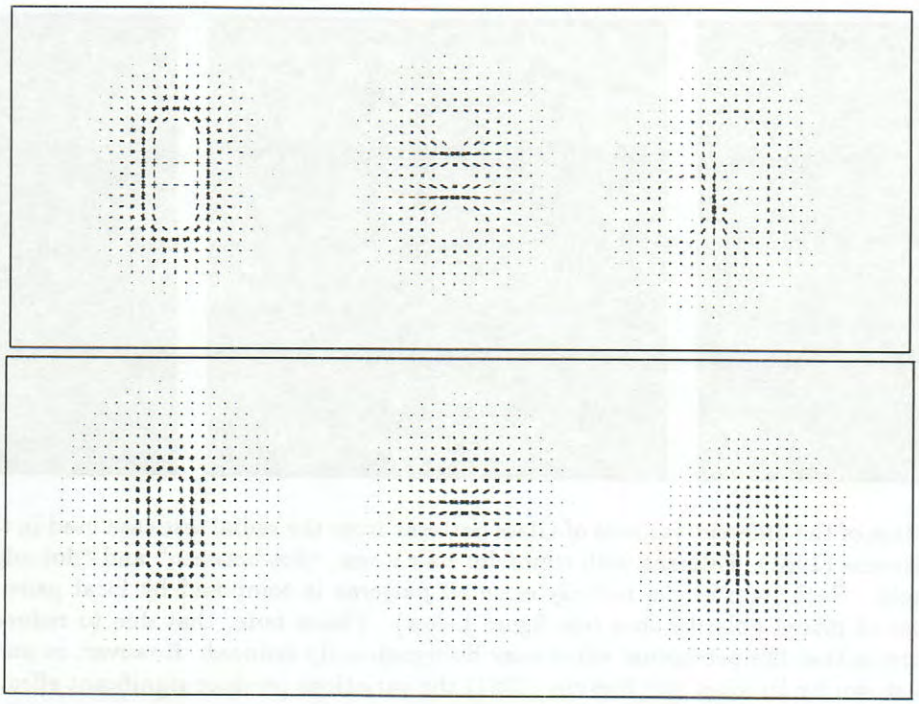

Figure 11: Results of processing the local items used by Brookes and Stevens (1991) to generate the Glass pattern variants. Results of processing for the three items (white dot pair, "dot-between", "dot-adjacent") are shown for the non-linear circuit (top row) and for the linear model (bottom row). For a better visualization of individual contributions for different orientations we show "needle" diagrams in which the activities for the spatial orientations are plotted at each location. The length of each oriented needle encodes the relative magnitude of response (the magnitudes are normalized with respect to the maximum response that appears in the display). The results indicate the individual dominances in orientation response that correspond with that of the perceptual appearence of the variants of Glass stimuli (see text).

where shallow gradients need to be discounted. In fact, we claim that processes of contrast measurement need to be considered from a broader perspective, one in which issues such as the determination of surface qualities, ratio processing, to name a couple, are adequately taken into account. Mechanisms *only* based on contrast amplitude measurements may be too limited to account for general processing needs.

The circuit for contrast detection produces non-zero responses whenever ON or OFF responses from initial center-surround processing are present. This allows the circuit to signal shallow luminance gradients as in the case of ramps or harmonic modulations. The sharpness of a luminance transition, as at a luminance edge, is encoded by the spatial juxtaposition of such ON and OFF responses. Relative to the sampling scale of the proposed mechanism the circuit registers any juxtaposed input configuration producing an extra strong response component with respect to the individual linear contributions.

The response properties of the circuit were embedded within the framework of scale-space processing, in particular the mechanism of scale selection. With reference to linear models of contrast processing based, for instance, on Gaussian derivatives we have specified conditions for the generation of absolute maximum scale-space responses and verified these results through specific computer experiments. We suggest that the representation generated by circuit is uniquely selective to intrinsic parameters of the luminance transition of a priori unknown width and height.

Relation to other proposals. Our scheme shares important features with other contrast measurement proposals including the well-known Marr and Hildreth (1980) edge detection proposal. Marr and Hildreth's main idea is that it is possible to detect edges by linking the outputs of ON and OFF center-surround cells (such as LGN cells) through a *logical* AND-gate. Such a scheme is based on the idea that spatially adjacent ON and OFF responses represent the infelction point of a sharp transition – thus the *zero-crossings* of its second

order derivative locate the edge transition (Poggio, 1983). A closer inspection at the process of zero-crossing detection indicates that it utilizes an oriented multiplicative combination of initial ON/OFF responses based on a simple first-order difference mechanism. The zero-crossing can be formalized using our previous notation used in Section 2. A light-dark (dark-light) transition is detected via

$$z^{LD} = \max\left[c^{+}_{i,j} \cdot c^{-}_{i+1,j}, c^{+}_{i,j} \cdot c^{-}_{i,j+1}\right] \quad \text{and}$$

$$z^{DL} = \max\left[c^{-}_{i,j} \cdot c^{+}_{i+1,j}, c^{-}_{i,j} \cdot c^{+}_{i,j+1}\right]$$

(compare with Equations 5, 6 and 15).

While our model provides a circuit capable of realizing an AND-gate like behavior, it does not compute a logical AND-gate, but instead a *soft* gate. This key property distinguishes the prepent proposal from the Marr and Hildreth method. Although important, edge detection should not be the sole aim of contrast measurement. As stated above, what is needed is a general, robust method of contrast measurement that incorporates not only physical contrast assessment, but also other factors, such as transition *form*. In addition, image contours are present not only at edges but at other luminance distributions (see, *e.g.*, Figure 8 of Pessoa (1996b)). Moreover, utilizing a numerical difference scheme, simple Fourier interpretation renders such a mechanism highly sensitive to noise. This is not the case in our model as we use Gaussian low-pass filters before sampling ON- and OFF-inputs.

In more general terms, the gating-like mechanisms for integrating activations from different sub-fields have their roots in early biologically inspired modeling for contrast detection in computational vision. The cascaded processing of input luminances by initial center-surround linear filtering followed by a non-linear step of zero-crossing detection (Marr and Hildreth, 1980; Marr, 1982) has received most visibility in the past. The non-linear step of detecting local sign-changes (zero-crossings) in the response of Laplacian-of-Gaussian filtering of the input luminance can be interpreted as a coarse approximation of the action of a cortical contrast cell that integrates both excitatory and inhibitory input branches by a gating-type operation (Richter and Ullman, 1986; Poggio, 1983). The analysis of the differential structure of image curves and contrast outlines lead Zucker and colleagues (Dobbins *et al.*, 1990; Iverson and Zucker, 1995) to propose a syntactic scheme defining a language of logical/linear operators. In this formalization, operators composed of tangentially separated sub-fields were designed to selectively respond to contrast ("edge") and line features while enabling the operators to automatically suppress "false" responses.

The characterizing feature of Zucker's logical/linear scheme is that it selectively suppresses any response that is generated by a luminance structure to which a contrast or line operator does not fit. Yet it generates the responses as a *linear* detection scheme but only show them for those locations that the *logical* scheme identifies as matching the filter's measurement competence. In our model we allow the circuit to signal the presence of relevant structure, such as the knees of a ramp, that appears as not perfectly matching the structure the circuit was designed for. In the case of a step transition, however, the presence of such a sharp contrast is signalled by an extra amount of high amplitude response that raises the activation over that of the linear response alone. This allows the decision as to what constitutes significant structure to be postponed, and in this way allow more global stages of visual integration to selectively focus and enhance visual structure that initially does not appear as dominant in matching amplitude response. In all, the non-linearities in Zucker's and in our scheme differ: in Zucker's approach the non-linearity functions as an early local *decision* mechanism, while in our model it serves as an *emphasizing*, or "boosting," mechanism to generate a high amplitude or energy response.

While these other computational models have not explicitly discussed any scale-space related processing properties, our scheme nicely generalizes to the multi-scale framework of edge detection. We have demonstrated how the non-linearity in the response to juxtaposed ON- and OFF-input can be utilized to signal the optimal operator scale for a gradual luminance transition of a certain spatial extent. The multi-scale scheme approximates a Gaussian first-order derivative scheme that makes use of the non-linearity in a scale-dependent input combination of adjacent contrast arrangement.

Simple cell physiology. Originating from Hubel and Wiesel's proposal, a long-standing view of simple cell response is that it depends on the *linear* sum of ON and OFF LGN signals (for a review see von der Heydt, 1987). In other words, simple cells linearly sum (or pool) all or their inputs – weighted by their effective strength which is defined by the RF response profile. Data supporting the view that simple cells behave as

linear devices come from a study by Schumer and Movshon (1984) showing that simple cells integrate their inputs in a sum-to-threshold linear manner. In addition, stimulus-response measurements of cells using spatial frequency modulated luminance gratings reveals a basically linear relationship whose sensitivity profile can be closely approximated by, among others, Gabor/Wavelet profiles generated by a Gaussian weighted sinusoidal spatial modulation (Pollen and Ronner, 1983; see Daugman, 1985, for a mathematical description), derivative of Gaussian profiles, or offset Gaussian profiles (Heggelund *et al.*, 1983).

Non-linearities utilized in several computational schemes, like ours, have also been observed in cortical simple cell behavior thus indicating that the view of such cells as linear devices is untenable (see von der Heydt, 1987). For example, Hammond and MacKay (1983) investigated the legth-summation characteristics and probed cells with bars composed of opposite polarity segments (i.e., light and dark segments). An OFF-subfield was probed by a dark bar that includes two light endings, and the same was done for the ON-subfield using light bars with dark segments at their end. The inclusion of inverse-polarity segments largely *suppresses* cell responses instead of only causing a reduction of response that is proportional to the length of the opposite polarity segments used – as predicted by the linearity assumption. A more recent investigation by von der Heydt *et al.* (1991) has demonstrated the existence in areas V1 and V2 of cells selectively responsive to oriented high spatial frequency gratings. Cells of this type vividly respond to gratings composed of alternating light and dark bars while remaining silent when stimulated by isolated bars of either contrast polarity. This has been interpreted as evidence for non-linear sub-field integration since the responses could not be reconciled with a linear filter model responsive to gratings of the given spatial frequency. The responses were critically dependent on the precise stimulus periodicity suggesting that the cells integrate spatially aligned arrangements of alternating ON and OFF LGN input in a non-linear way (see von der Heydt (1987) for an overview and discussion of previous findings in that direction, and Petkov and Kruizinga (1997) for an approach to model the key behavior).

These and several other observations suggest that the view of cortical contrast selective cells as being basically linear devices is too reductionistic. In addition, there is growing evidence that they are sensitive to more than just local contrast magnitude. We suggest that an analysis based on a broader view of the functionality of early stages in visual processing may guide the development of models of visual contrast measurement.

References

Arend, L. and Goldstein, R. (1987). Lightness models, gradient illusions, and curl. *Perception & Psychophysics*, **42**, 65-80.

Blake, A. (1985). Boundary conditions for lightness computation in Mondrian world. *Comp. Vis., Graph., and Image Process.*, **32**, 314-327.

Bracewell, R.N. (1978). *The Fourier transform and its applications* (Ed.2). McGraw-Hill, New York.

Brookes, R.A. and Stevens, K.A. (1991). Symbolic grouping versus simple cell models. *Biol. Cybern.*, **65**, 375-380.

Buf, J. du (1993). Responses of simple cells: Events, interferences, and ambiguities. *Biol. Cybern.*, **68**, 321-333.

Buf, J. du (1994). Ramp edges, Mach bands, and the functional significance of the simple cell assembly. *Biol. Cybern.*, **69**, 449-461.

Carandini, M. and Heeger, D.J. (1994). Summation and division by neurons in primate visual cortex. *Science*, **264**, 1333-1336.

Daugman, J. (1985). Uncertainty relation for resolution in space, spatial frequency, and orientation optimized by two-dimensional visual cortical filters. *J. Opt. Soc. of America*, **A,2**, 1160-1169.

Dobbins, A.L., Iverson, L., and Zucker, S.W. (1990). A logical/linear model of cortical subunit interaction. *Proc. ARVO'90 (Invest. Ophtal. and Vis. Sci., 31(4), PGM# 1954-95)*, 397, Sarasota, Florida (USA), Apr.29 - May 4.

Enroth-Cugell, C. and Robson, J.G. (1966). The contrast sensitivity of retinal ganglion cells of the cat. *J. Physiol.*, **187**, 517-552.

Ferster, D. (1988). Spatially opponent excitation and inhibition in simple cells of the cat visual cortex. *J. Neurosci.*, 8(4), 1172-1180.

Ferster, D. (1989). The synaptic inputs to simple cells in the cat visual cortex. In D. Lam and C. Gilbert (Eds.), *Neural mechanisms of visual perception*, ch. 3, 63-85. Portfolio Publ. Co., The Woodlands, Texas.

Furman, G.G. (1965). Comparison of for subtractive and shunting lateral-inhibition in receptor-neuron fields. *Kybernetik*, **2**, 257-274.

Glass, L. (1969). Moiré effect from random dots. *Nature*, **223**(5206), 578-580.

Grossberg, S. (1970). Neural pattern discrimination. *J. of Theor. Biol.*, **27**, 291-337.

Grossberg, S. and Mingolla, E. (1985). Neural dynamics of form perception: Boundary completion, illusory contours, and neon color spreading. *Psychol. Rev.*, **92**(2), 173-211.

Hammond, P. and MacKay, D. (1983). Influence of luminance gradient reversal on simple cells in feline striate cortex. *J. Physiol.*, **337**, 69-87.

Heggelund, P. (1981). Receptive field organization of simple cells in cat striate cortex. *Exp. Brain Res.*, **42**, 89-98.

Heggelund, P. (1986). Quantitative studies of enhancement and suppression zones in the receptive field of simple cells in cat striate cortex. *J. Physiol.*, **373**, 293-310.

Heggelund, P., Krekling, S., and Skottun, B.C. (1983). Spatial summation in the receptive field of simple cells in the cat striate cortex. *Exp. Brain Res.*, **52**, 87-98.

Hodgkin, A.L. (1964). *The conduction of the nervous impulse*. Liverpool University Press, Liverpool.

Horn, B.K.P. (1974). Computing lightness from an image. *Comp. Graph. and Image Process.*, **3**, 277-299.

Hubel, D.H. and Wiesel, T.N. (1962). Receptive fields, binocular interaction and functional architecture in the cat's visual cortex. *J. Physiol.*, **160**, 106-154.

Iverson, L.A. and Zucker, S.W. (1995). Logical/linear operators for image curves. *IEEE Trans. on PAMI*, **17**(10), 982-996.

Koenderink, J.J. (1984). The structure of images. *Biol. Cybern.*, **50**, 363-370.

Koenderink, J.J. and van Doorn, A. (1990). Receptive field families. *Biol. Cybern.*, **63**, 291-297.

Land, E.H. and McCann, J.J. (1971). Lightness and retinex theory. *J. Opt. Soc. Amer.*, **61**, 1-11.

Lindeberg, T. (1996). Scale-space: A framework for handling image structures at multiple scales. Lecture notes from *The CERN School of Computing 1996*, Egmond aan Zee (NL), Sept.8-21. (`ftp://ftp.bion.kth.se/reports/lin-cern-summ-school-96.ps.Z`).

Lindeberg, T. and ter Haar Romeny, B. (1994). Linear scale-space I: Basic theory. In B. ter Haar Romeny (Ed.), *Geometry-Driven Diffusion in Computer Vision*, 1-38. London, Freund Publ. House Ltd.

Liu, Z., Gaska, J.P., Jacobson, L.D., and Pollen, D.A. (1992). Interneuronal interaction between members of quadrature phase and anti-phase pairs in the cat's visual cortex. *Vision Research*, **32**(7), 1193-1198.

Marr, D. (1982). *Vision*, San Francisco, W.H. Freeman & Co.

Marr, D. and Hildreth, E. (1980). Theory of edge detection. *Proc. Royal Soc. of London (B)*, **207**, 187-217.

Morrone, M.C. and Burr, D.C. (1988). Feature detection in human vision: A phase-dependent energy model. *Proc. Royal Soc. of London (B)*, **235**, 221-245.

Morrone, M.C., Burr, D.C., and Maffei, L. (1982). Functional implications of cross-orientation inhibition of cortical visual cells. I. Neurophysiological evidence. *Proc. Royal Soc. of London (B)*, **216**, 335-354.

Neumann, H. (1993). Toward a computational architecture for unified visual contrast and brightness perception: I. Theory and model. *Proc. of the World Congr. on Neural Networks* (WCNN-93), Portland, Oregon (USA), Vol. I-IV, (I)84-91. LEA.

Neumann, H. (1996). Mechanisms of neural architecture for visual contrast and brightness perception. *Neural Networks*, **9**(6), 921-936.

Neumann, H. and Ottenberg, K. (1992a). Estimating ramp-edge attributes from scale-space. In J. Vandevalle, R. Boite, M. Moonen, and A. Oosterlinck. *Signal Processing VI: Theories and Applications*, Vol. I - III, (6th Europ. Signal Proc. Conf. (EUSIPCO-92), ICPR-92), Brussels (Belgium), (I)603-607. Elsevier.

Neumann, H. and Ottenberg, K. (1992b). Estimating attributes of smooth signal transitions from scale-space. *Proc. 11th Int. Conf. on Pattern Recognition* (ICPR-92), The Hague (NL), Vol.I-IV, (III)754-758. IEEE Press.

Neumann, H. and Pessoa, L. (1994). A simple cell model with multiple spatial frequency selectivity and linear/non-linear response properties. *Proc. of the World Congr. on Neural Networks* (WCNN-94), San Diego, Calif. (USA), Vol. I-IV, (IV)290-298. LEA.

Pessoa, L. (1996a). Mach band attenuation by adjacent stimuli: Experiment and filling-in simulations. *Perception*, **25**, 425-442.

Pessoa, L. (1996b). Mach bands: How many models are possible? Recent experimental findings and modeling attempts. *Vision Research*, **36**, 3205-3227.

Pessoa, L., Mingolla, E., and Neumann, H. (1995). A contrast- and luminance-driven multiscale network model of brightness perception. *Vision Research*, **35**, 2201-2223.

Petkov, N. and Kruizinga, P. (1997). Computational models of visual neurons specialised in the detection of periodic and aperiodic oriented visual stimuli: Bar and grating cells. *Biol. Cybern.*, **76**, 83-96.

Poggio, T. (1983). Visual algorithms. In O.J. Braddick and A.C. Sleigh (Eds.), *Physical and Biological Processing of Images*, Vol. 11 of Springer Series in Information Sciences, 128-153. Springer.

Pollen, D.A. and Ronner, S.F. (1983). Visual cortical neurons as localized spatial frequency filters. *IEEE Trans. on SMC*, **13**(5), 907-916.

Richter, J. and Ullman, S. (1986). Non-linearities in cortical simple cells and the possible detection of zero-crossings. *Biol. Cybern.*, **53**, 195-202.

Rodieck, R.W. (1965). Quantitative analysis of cat retinal ganglion cell responses to visual stimuli. *Vision Research*, **5**, 583-601.

Sagi, D., Kovács, L., and Eötvös, L. (1993). Long range processes involved in the perception of Glass patterns. *Proc. ARVO'93 (Invest. Ophtal. and Vis. Science, 34(4), PGM# 2106)*, 1130, Sarasota, Florida (USA), May 2 - 7.

Schiller, P. (1992). The ON and OFF channels of the visual system. *Trends in Neurosci.*, **15**(3), 86-91.

Schumer, R.A. and Movshon, J.A. (1984). Length summation in simple cells in cat striate cortex. *Vision Research*, **24**(6), 565-571.

Tolhurst, D.J. and Dean, A.F. (1990). The effects of contrast on the linearity of spatial summation of simple cells in the cat's striate cortex. *Exp. Brain Res.*, **79**, 582-588.

Vidyasagar, T.R., Pei, X., and Volgushev, M. (1996). Multiple mechanisms underlying the orientation selectivity of visual cortical neurones. *Trends in Neurosci.*, **19**(7), 272-277.

von der Heydt, R. (1987). Approaches to visual cortical function. *Rev. Physiol. Biochem. Pharmacol.*, **108**, 69-150.

von der Heydt, R., Peterhans, E., and Dürsteler, M.R. (1991). Grating cells in monkey visual cortex: Coding texture? In B. Blum (Ed.), *Channels in the Visual Nervous System: Neurophysiology, Psychophysics and Models*, 53-73. London, Freund Publ. House Ltd.

Witkin, A.P. (1983). Scale-space filtering. *Proc. 8th Int. Joint Conf. on Artificial Intelligence*, IJCAI-83, Vol.I-II, (II)1019-1022, Karlsruhe (FRG).

Appendix 1: A Linear Gaussian Edge Detector in Scale-Space

This section draws upon previous work by Neumann and Ottenberg (1992a,b) who investigated finding the optimum scale-space response for 1D odd-symmetric intensity transitions based on a linear pre-processing stage. In particular, we utilize here the cascade processing of the initial center-surround processing stage followed by an operation that realizes a low-pass filtered 1st order derivative. We use an oriented gauge coordinate system (u, v) as introduced above in order to express the derivative attributes in terms of matched directional derivative operations. We utilize this framework to relate the findings on the evolution of scale-space response to the concept of *automatic scale selection*, which has only recently been suggested by Lindeberg (1996)[7]. It should be noted that for the analysis of scale-space response we only analyze here the numerator term of the normalized response. Since we further investigate the relation between linear and non-linear response in relation to their scale-selection properties (see Appendix 2), the denominator component for normalization was omitted here. We start with the analysis of response to a step edge and then proceed to the more general case of a ramp transition.

Response for a step edge luminance transition. A step edge profile of height h defined by an amplitude-scaled Heaviside function, thus having

$$f_{step}(u) = h \cdot \mathcal{H}(u).$$

The model consists of a sequence of principal processing stages. The first step consists of a center-surround mechanism defining an isotropic band-pass filtering operation. We approximate the (normalized) difference-of-Gaussian (see Equation 3) by a Laplacian-of-Gaussian (LoG) operation. The response is generated by the spatial convolution of the step profile with the impulse response of the LoG-filter, $f_{step}(u) \otimes \mathrm{LoG}_\sigma(u)$. We get[8]

$$\mathrm{LoG}_{step}(u) = h \frac{d}{du} \mathrm{G}_\sigma(u).$$

The LoG-filtered profile is processed subsequently by a 1st order (Gaussian) derivative ($D1G$) filter. In its limits, for $\sigma \to 0$, the Gaussian derivative will converge to $d/du\, \delta(u)$. The final spatial profile of contrast cell responses for its minimum spatial scale limits is given by

$$s_{\mathrm{step}}(u) = h \cdot \frac{d^2}{du^2} \mathrm{G}_\sigma(u) = \frac{h}{\sigma^2} \left[1 - \frac{u^2}{\sigma^2} \right] \mathrm{G}_\sigma(u).$$

The response amplitude at the step edge location, $u = 0$, for a normalized Gaussian weighting function is then

$$s_{\mathrm{step}}(u = 0) = \left| \frac{h}{\sigma^2} \mathrm{G}_\sigma(u) \right| = \left| \frac{h}{\sqrt{2\pi} \cdot \sigma^3} \right|.$$

The result shows that the response taken as a function of scale σ is strong monotonically decreasing such that the maximum response appears for the smallest scale.

Response for a ramp edge luminance transition. A ramp edge profile of width R and height h can be generated by the convolution of an amplitude-scaled Heaviside function (see above) with a unit-pulse function of the corresponding width. The profile is thus described analytically as

$$f_{ramp}(u) = h \cdot \mathcal{H}(u) \otimes \Pi_R(u).$$

The response of the model is generated by the spatial convolution of the ramp profile with the impulse response of the LoG-filter, $f_{ramp}(u) \otimes \mathrm{LoG}_\sigma(u)$. We get

$$\mathrm{LoG}_{ramp}(u) = \frac{h}{R} \left(\mathrm{G}_\sigma(u + \frac{R}{2}) - \mathrm{G}_\sigma(u - \frac{R}{2}) \right).$$

[7] Thanks to Maria Quiteria for providing some of the insights and a fresh view on recent modeling approaches.

[8] For simplicity, we are neglecting the fact that for this 2D isotropic pre-filtering stage the effective space constant is $\sigma_e = \sqrt{2}\sigma$. Since this refers only to a rescaling of coordinate axes, we further deal with the original scale constant σ only.

Corresponding to the procedure we have adopted for the step case, further processing of the LoG-filtered profile by a 1st order (Gaussian) derivative ($D1G$) filter yields

$$s_{\text{ramp}}(u) = \frac{h}{R}\left(\frac{d}{du}\mathrm{G}_\sigma(u+\frac{R}{2}) - \frac{d}{du}\mathrm{G}_\sigma(u-\frac{R}{2})\right).$$

As one can see, the response consists of a sum of two Gaussian derivative profiles of opposite sign shifted to either side of the central location of the ramp transition. For completeness, we can confirm the result to include the special case of a step transition. By taking the limit $R \to 0$ the response $s_{\text{ramp}}(u)$ converges to that derived for a step, $\lim_{R\to 0} s_{\text{ramp}}(u) = s_{\text{step}}(u)$ (see above).

Scale-space processing and responses at ramp edge location. Depending on the width of the ramp and the relative scaling of the cascaded pre-processing stage, the response profile appears in different spatial arrangement. We consider a case that has been sketched in Fig. 4. For a scale that is small relative to the transition width ($\sigma \ll R$), Gaussian derivatives appear as isolated ON and OFF channel responses at the knees where the plateaus meet the ramp transition. For a coarser scale after blurring, the central lobes of either ON or OFF response (depending on a light-dark or a dark-light transition, respectively) meet and overlap at the center of the ramp and appear as juxtaposed input contrast responses. Analytically, for a condition $R \ll \sigma$ (corresponding to $R \to 0$), we will get the 2nd order derivative of a Gaussian profile that peaks at the center of the ramp (compare with the results of mathematical investigation above and see Fig.6).

In order to evaluate the behavior of a scale-space edge detector for a gradual luminance transition, we watch its response at the center of the ramp ($u = 0$). For that we make use of the even-symmetry of the Gaussian, such that we finally get the amplitude

$$s_{\text{ramp}}(u=0) = 2\frac{h}{R}\cdot \mathrm{G}'_\sigma(\frac{R}{2}).$$

We now treat s_{ramp} as a function of scale σ such that we derive the magnitude function

$$s_{\text{ramp}}(\sigma)|_{u=0} = \frac{h}{\sqrt{2\pi}\sigma^3}\exp\left[-\frac{R^2}{8\sigma^2}\right].$$

Figure 12 shows profiles of scale-space responses of a linear cell for variable parameter settings of ramp transition

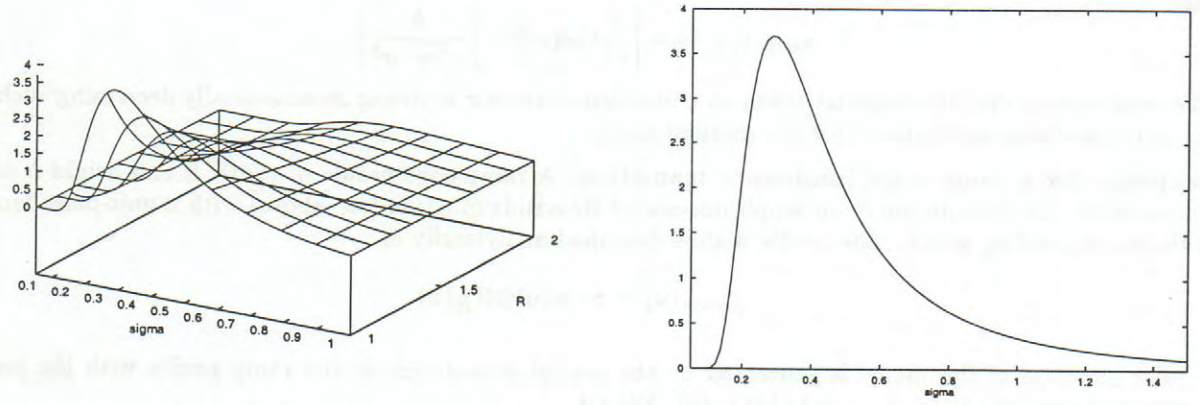

Figure 12: Linear contrast cell response at ramp location $u = 0$ treated as a function of scale (σ). Processing results of a family of ramp profiles of unit height ($h = 1$) is shown as a surface for different widths R (left); the shape of the response profile for one fixed setting of R shows a unique maximum in response as a function of scale (right). As it is predicted by the equation for $s_{\text{ramp}}(\sigma)|_{u=0}$, a unique shape of scale-space profiles is shifted in peak location for increasing values of R accompanied by a drop in overall response amplitude.

widths R and constant height $h = 1$. The responses for a ramp transition shown in Section 4 (Fig. 6 (bottom))

represent a coarse sample of the analytic profile presented in Fig. 12 (right). For a mechanism capable to select an appropriate scale it needs a proper selection and decision criterion. A useful candidate for this selection appears to be the maximum scale response along $u = 0$. The unique peak response along scale is determined by the zero-crossing of the slope function for $s_{\text{ramp}}(\sigma)|_{u=0}$. We get

$$\frac{d}{d\sigma} s_{\text{ramp}}(\sigma) = -\frac{h}{\sqrt{2\pi}\sigma^4} \left(\frac{R^2}{4\sigma^2} - 3 \right) \exp\left[-\frac{R^2}{8\sigma^2} \right] = 0.$$

The solution for the scale-space location of the peak response is given by

$$\sigma_{max} = \frac{R}{2\sqrt{3}},$$

which indicates an operator scaling slightly less than half the ramp transition width. A mechanism reading out such maximum responses must rely on a robust selection criterion that guarantees the correspondence with a representation of variable-width contrast edges. We investigate this topic below in terms of absolute maximum contrast responses suggesting a winner-take-all type mechanism.

Scale selection for a ramp contrast. In order to investigate the relevant conditions for selecting maximal responses corresponding to a ramp of certain width, we compare the activations generated for $s_{\text{ramp}}(\sigma_{max})|_{u=0} \equiv s_{\text{ramp}}(u = 0)|_{\sigma=\sigma_{max}}$ with the absolute height of one lobe in the profile of $D1\text{G}$. In particular, we investigate the response for $s_{\text{ramp}}(u = -R/2 + \sigma_0)$. The latter corresponds to the case of isolated constrast responses at the knees of the ramp that are processed by the $D1\text{G}$ filter. For the condition $\sigma_0 \ll R$ the response profile in u-direction shows

$$s_{\text{ramp}}(u = -R/2 + \sigma_0)|_{\sigma_0 \ll R} = \frac{h}{R} \left[\frac{d}{du} \text{G}_\sigma(\sigma_0) - \underbrace{\frac{d}{du} \text{G}_\sigma(-R + \sigma_0)}_{\approx 0} \right]$$

(see Fig. 6 (bottom, left) for comparison). Since the second derivative term almost vanishes we can simplify the equations by only considering the dominant component for further analysis. This condition corresponds to a situation where $\sigma_0 < \sigma_{max}$ holds. If we compare the responses of the two selected cases we get

$$\begin{aligned} s_{\text{ramp}}(u = 0)|_{\sigma=\sigma_{max}} &= \frac{48\sqrt{3}h}{\sqrt{2\pi}} \exp\left[-\frac{3}{2} \right] \cdot \frac{1}{R^3} \\ s_{\text{ramp}}(u = -R/2 + \sigma_0)|_{\sigma_0 \ll R} &\approx \frac{h}{\sqrt{2\pi}} \exp\left[-\frac{1}{2} \right] \cdot \frac{1}{R\sigma^2} \end{aligned}$$

With the ratio of these two expression we get a condition for *absolute* maximum response. For that purpose we introduce the normalized scale-space variable $\hat{\sigma} = \sigma/R$. The condition then finally reads

$$\begin{aligned} \frac{48\sqrt{3}}{e} \hat{\sigma}^2 &> 1 \qquad \text{or, equivalently} \\ \hat{\sigma} &> \sqrt{\frac{e}{48\sqrt{3}}} \approx 0.18, \qquad \text{with} \quad e = \exp[1]. \end{aligned}$$

We left the first version of the inequality for direct comparison with the result derived for the non-linear circuit (Appendix 2).

The result for the linear model demonstrates that the identified optimum scale is not guaranteed to yield maximum responses in absolute terms as related to the overall field of activities. In particular, if $\hat{\sigma}$ becomes less than approximately 1/5, the response $s_{\text{ramp}}(u = 0)|_{\sigma=\sigma_{max}}$ already declined to a value lower than the maximum response for the smallest scale, as demonstrated in Fig. 6 (bottom). If, however, the necessary condition is met, the maximum scale response determines the overall maximum amplitude in the array of scale-space filter responses.

Appendix 2: Scale-Space Response for the Non-Linear Circuit

It has been shown in Appendix 1 that the linear model already shows a selectivity for an optimal scale. The response taken as a function of scale $S(\sigma)$ yields a unique maximum value, prerequisite for automatic scale selection. However, it was shown that this value cannot be guaranteed to be the maximum response in absolute terms – as also demonstrated by the simulations shown in Fig. 6.

A compact notation of the response properties of the non-linear circuit is given by

$$z = \mathcal{L} \cdot \left((p^+ + p^-) + \frac{\mathcal{N}}{\mathcal{L}} \cdot (p^+ \cdot p^-) \right)$$

(compare with Equation 16). This demonstrates that the non-linear circuit in its linear processing behavior inherits all qualitative properties shown in Appendix 1. The more, for configurations approaching the optimum scale conditions, i.e. configurations with juxtaposed ON and OFF activations, the results of the linear processing component are superimposed by the correlation (gating) between ON and OFF responses.

The function $\mathcal{L}$ only defines a proportionality for both linear and non-linear components. For any further analysis of the response z, it is therefore sufficient to consider the terms in large brackets (see equation above). The non-linear contribution is scaled by the factor $\mathcal{N}/\mathcal{L}$. Since we want to relate the cell response to the activations generated by the initial center-surround processing stage, we have to scale this ratio accordingly. Based on the dependency described in Equation 5 we arrive at

$$\mathcal{N}' \equiv \frac{\mathcal{N}}{\mathcal{L}} (\beta_s + \delta_s) = 2 \frac{\beta_c}{\alpha_c} (\beta_s + \delta_s),$$

in which $(\beta_s + \delta_s)$ is the gain of the initial center-surround processing stage, denoted by $net^{\pm} - net^{\mp}$.

Non-linear response for step edges. In Appendix 1 we have analyzed the responses of a linear mechanism processing a step edge profile. The non-linear part of the total response is constributed by $(p^+ \cdot p^-)$. We determine the magnitudes from the maxima in the $D1G$ profile. These correspond to the offset points for sub-field integration given by $\tau = \pm\sigma$. For the profile of a 1st derivative of a Gaussian we get

$$h \frac{d}{du} \mathrm{G}_\sigma(u = \sigma) = -\frac{h}{\sqrt{2\pi\sigma^2}} \exp\left[-\frac{1}{2}\right].$$

We introduce the functions ${s_{\mathrm{step}}}^{lin} \equiv s_{\mathrm{step}}$ (see Appendix 1) and ${s_{\mathrm{step}}}^{nl}$ and show the non-linear response in terms of the linear response derived in Appendix 1. The significant part of a step edge response (proportion of response z given in brackets, see above) generated by the non-linear circuit is then given by

$$\begin{aligned} {s_{\mathrm{step}}}^{nl}(u = 0) &= \frac{h}{\sqrt{2\pi}\sigma^3} + \mathcal{N}' \frac{1}{\sqrt{2\pi}e\sigma}, \\ &= {s_{\mathrm{step}}}^{lin}(u = 0) \cdot \left(1 + \mathcal{N}' \frac{1}{\sqrt{2\pi}e\sigma} \right). \end{aligned}$$

Two observations can be made from this result: *(i)* as in the linear case, the response for a step edge is a monotonically decreasing function of scale in which the maximum response is generated at the smallest scale, and *(ii)* the contribution of the non-linearity dominates for a gain factor

$$\mathcal{N}' \gg \sqrt{2\pi}e\sigma.$$

Optimum input conditions for non-linear processing. Non-zero correlation between ON and OFF channel activation is available when both sub-fields of a cell integrate positive input activation. The initial center-surround responses at the knees of the ramp (see Appendix 1) therefore have to be progressively blurred to meet at the center of the ramp. For each Gaussian bump in the initial $\mathrm{LoG}_{ramp}(u)$ profile we get

$$\frac{h}{R} \left(\pm \mathrm{G}_{\sigma_0}(u \pm \frac{R}{2}) \otimes \mathrm{G}_\sigma(u) \right) = \pm \frac{h}{R} \mathrm{G}_{\sqrt{\sigma_0^2 + \sigma^2}}(u \pm \frac{R}{2}).$$

Proper scaling of the blurred profile approaches the value determined for the optimum scale, such that $\sqrt{\sigma_0^2 + \sigma^2} = \sigma_{max}$. The profile showing the difference of two broadly tuned offset Gaussians assembles a $D1G$ filter.

Input integration and maximum scale response for ramp edges. Since offsets were symmetric around the center of the ramp we sample each shifted Gaussian $G_{\sigma_{max}}(u \pm R/2)$ at $u = \pm\tau = \pm R/2$. For the gating-type input to the non-linear response we therefore get

$$(p^+ \cdot p^-)\,|_{\sigma=\sigma_{max}} = \frac{h^2}{R^2} \cdot \frac{1}{2\pi \cdot \sigma_{max}^2} = \frac{6h^2}{\pi \cdot R^4},$$

with $\sigma_{max} = R/(2\sqrt{3})$. We can now write the response amplitude of the non-linear circuit at the optimum scale condition, σ_{max}, as a combination of the linear (additive) and non-linear (correlational) input contribution. We introduce the functions ${s_{\text{ramp}}}^{lin} \equiv s_{\text{ramp}}$ (see Appendix 1) and ${s_{\text{ramp}}}^{nl}$ and present the non-linear response in terms of the linear response derived in Appendix 1. We get

$$\begin{aligned} {s_{\text{ramp}}}^{nl}(u=0)|_{\sigma=\sigma_{max}} &= \frac{48\sqrt{3}h}{\sqrt{2\pi}} \exp\left[-\frac{3}{2}\right] \cdot \frac{1}{R^3} + \mathcal{N}' \frac{6h^2}{\pi \cdot R^4}, \\ &= {s_{\text{ramp}}}^{lin}(u=0)|_{\sigma=\sigma_{max}} \cdot \left(1 + \mathcal{N}' \frac{\sqrt{2}}{8\sqrt{3\pi}} \frac{h}{R} \exp\left[\frac{3}{2}\right]\right). \end{aligned}$$

Several observations can be made from this result: *(i)* the response of the circuit for a ramp edge transition can be predicted for an optimum scale, *(ii)* the contribution of the non-linearity depends on the slope of the ramp transition denoted as $m = h/R$, *(iii)* the plain non-linearity of the circuit (without the gain $\mathcal{N}'$) contributes with a 26% increase – times the slope – in output magnitude. In the case of discrete signals and images any transitions are of unit width at minimum, i.e. $R \geq 1$. For a ramp of unit slope the non-linear component to dominate the response the gain factor $\mathcal{N}'$ has to be high enough to "boost" the output activation. Moreover, with such a gain factor it can be guaranteed that the magnitude of response is maximal in absolute terms (compare the analysis for a linear filter in Appendix 1). A dominance of the response caused by the non-linear, i.e. multiplicative, contribution from both ON and OFF sub-field is achieved for

$$\mathcal{N}' \gg 4\sqrt{6\pi} \frac{R}{h} \exp\left[-\frac{3}{2}\right].$$

Since the signal parameters h and R are not known in advance, the gain $\mathcal{N}'$ may be chosen high enough to guarantee the dominance of any non-linear contribution.

Liste der bisher erschienenen Ulmer Informatik-Berichte

Einige davon sind per FTP von `ftp.informatik.uni-ulm.de` erhältlich
Die mit * markierten Berichte sind vergriffen

List of technical reports published by the University of Ulm

Some of them are available by FTP from `ftp.informatik.uni-ulm.de`
Reports marked with * are out of print

91-01 *Ker-I Ko, P. Orponen, U. Schöning, O. Watanabe*
Instance Complexity

91-02* *K. Gladitz, H. Fassbender, H. Vogler*
Compiler-Based Implementation of Syntax-Directed Functional Programming

91-03* *Alfons Geser*
Relative Termination

91-04* *J. Köbler, U. Schöning, J. Toran*
Graph Isomorphism is low for PP

91-05 *Johannes Köbler, Thomas Thierauf*
Complexity Restricted Advice Functions

91-06* *Uwe Schöning*
Recent Highlights in Structural Complexity Theory

91-07* *F. Green, J. Köbler, J. Toran*
The Power of Middle Bit

91-08* *V.Arvind, Y. Han, L. Hamachandra, J. Köbler, A. Lozano, M. Mundhenk, A. Ogiwara, U. Schöning, R. Silvestri, T. Thierauf*
Reductions for Sets of Low Information Content

92-01* *Vikraman Arvind, Johannes Köbler, Martin Mundhenk*
On Bounded Truth-Table and Conjunctive Reductions to Sparse and Tally Sets

92-02* *Thomas Noll, Heiko Vogler*
Top-down Parsing with Simulataneous Evaluationof Noncircular Attribute Grammars

92-03 *Fakultät für Informatik*
17. Workshop über Komplexitätstheorie, effiziente Algorithmen und Datenstrukturen

92-04* *V. Arvind, J. Köbler, M. Mundhenk*
Lowness and the Complexity of Sparse and Tally Descriptions

92-05* *Johannes Köbler*
Locating P/poly Optimally in the Extended Low Hierarchy

92-06* *Armin Kühnemann, Heiko Vogler*
Synthesized and inherited functions -a new computational model for syntax-directed semantics

92-07* *Heinz Fassbender, Heiko Vogler*
A Universal Unification Algorithm Based on Unification-Driven Leftmost Outermost Narrowing

92-08* *Uwe Schöning*
On Random Reductions from Sparse Sets to Tally Sets

92-09* *Hermann von Hasseln, Laura Martignon*
Consistency in Stochastic Network

92-10 *Michael Schmitt*
A Slightly Improved Upper Bound on the Size of Weights Sufficient to Represent Any Linearly Separable Boolean Function

92-11 *Johannes Köbler, Seinosuke Toda*
On the Power of Generalized MOD-Classes

92-12 *V. Arvind, J. Köbler, M. Mundhenk*
Reliable Reductions, High Sets and Low Sets

92-13 *Alfons Geser*
On a monotonic semantic path ordering

92-14* *Joost Engelfriet, Heiko Vogler*
The Translation Power of Top-Down Tree-To-Graph Transducers

93-01 *Alfred Lupper, Konrad Froitzheim*
AppleTalk Link Access Protocol basierend auf dem Abstract Personal Communications Manager

93-02 *M.H. Scholl, C. Laasch, C. Rich, H.-J. Schek, M. Tresch*
The COCOON Object Model

93-03 *Thomas Thierauf, Seinosuke Toda, Osamu Watanabe*
On Sets Bounded Truth-Table Reducible to P-selective Sets

93-04 *Jin-Yi Cai, Frederic Green, Thomas Thierauf*
On the Correlation of Symmetric Functions

93-05 *K.Kuhn, M.Reichert, M. Nathe, T. Beuter, C. Heinlein, P. Dadam*
A Conceptual Approach to an Open Hospital Information System

93-06 *Klaus Gaßner*
Rechnerunterstützung für die konzeptuelle Modellierung

93-07 *Ullrich Keßler, Peter Dadam*
Towards Customizable, Flexible Storage Structures for Complex Objects

94-01 *Michael Schmitt*
On the Complexity of Consistency Problems for Neurons with Binary Weights

94-02 *Armin Kühnemann, Heiko Vogler*
A Pumping Lemma for Output Languages of Attributed Tree Transducers

94-03 *Harry Buhrman, Jim Kadin, Thomas Thierauf*
On Functions Computable with Nonadaptive Queries to NP

94-04 *Heinz Faßbender, Heiko Vogler, Andrea Wedel*
Implementation of a Deterministic Partial E-Unification Algorithm for Macro Tree Transducers

94-05 *V. Arvind, J. Köbler, R. Schuler*
On Helping and Interactive Proof Systems

94-06 *Christian Kalus, Peter Dadam*
Incorporating record subtyping into a relational data model

94-07 *Markus Tresch, Marc H. Scholl*
A Classification of Multi-Database Languages

94-08 *Friedrich von Henke, Harald Rueß*
Arbeitstreffen Typtheorie: Zusammenfassung der Beiträge

94-09 *F.W. von Henke, A. Dold, H. Rueß, D. Schwier, M. Strecker*
Construction and Deduction Methods for the Formal Development of Software

94-10 *Axel Dold*
Formalisierung schematischer Algorithmen

94-11 *Johannes Köbler, Osamu Watanabe*
New Collapse Consequences of NP Having Small Circuits

94-12 *Rainer Schuler*
On Average Polynomial Time

94-13 *Rainer Schuler, Osamu Watanabe*
Towards Average-Case Complexity Analysis of NP Optimization Problems

94-14 *Wolfram Schulte, Ton Vullinghs*
Linking Reactive Software to the X-Window System

94-15 *Alfred Lupper*
Namensverwaltung und Adressierung in Distributed Shared Memory-Systemen

94-16 *Robert Regn*
Verteilte Unix-Betriebssysteme

94-17 *Helmuth Partsch*
Again on Recognition and Parsing of Context-Free Grammars:
Two Exercises in Transformational Programming

94-18 *Helmuth Partsch*
Transformational Development of Data-Parallel Algorithms: an Example

95-01 *Oleg Verbitsky*
On the Largest Common Subgraph Problem

95-02 *Uwe Schöning*
Complexity of Presburger Arithmetic with Fixed Quantifier Dimension

95-03 *Harry Buhrman, Thomas Thierauf*
The Complexity of Generating and Checking Proofs of Membership

95-04 *Rainer Schuler, Tomoyuki Yamakami*
Structural Average Case Complexity

95-05 *Klaus Achatz, Wolfram Schulte*
Architecture Indepentent Massive Parallelization of Divide-And-Conquer Algorithms

95-06 *Christoph Karg, Rainer Schuler*
Structure in Average Case Complexity

95-07 *P. Dadam, K. Kuhn, M. Reichert, T. Beuter, M. Nathe*
ADEPT: Ein integrierender Ansatz zur Entwicklung flexibler, zuverlässiger kooperierender Assistenzsysteme in klinischen Anwendungsumgebungen

95-08 *Jürgen Kehrer, Peter Schulthess*
Aufbereitung von gescannten Röntgenbildern zur filmlosen Diagnostik

95-09 *Hans-Jörg Burtschick, Wolfgang Lindner*
On Sets Turing Reducible to P-Selective Sets

95-10 *Boris Hartmann*
Berücksichtigung lokaler Randbedingung bei globaler Zieloptimierung mit neuronalen Netzen am Beispiel Truck Backer-Upper

95-12 *Klaus Achatz, Wolfram Schulte*
Massive Parallelization of Divide-and-Conquer Algorithms over Powerlists

95-13 *Andrea Mößle, Heiko Vogler*
Efficient Call-by-value Evaluation Strategy of Primitive Recursive Program Schemes

95-14 *Axel Dold, Friedrich W. von Henke, Holger Pfeifer, Harald Rueß*
A Generic Specification for Verifying Peephole Optimizations

96-01 *Ercüment Canver, Jan-Tecker Gayen, Adam Moik*
Formale Entwicklung der Steuerungssoftware für eine elektrisch ortsbediente Weiche mit VSE

96-02 *Bernhard Nebel*
Solving Hard Qualitative Temporal Reasoning Problems: Evaluating the Efficiency of Using the ORD-Horn Class

96-03 *Ton Vullinghs, Wolfram Schulte, Thilo Schwinn*
An Introduction to TkGofer

96-04 *Thomas Beuter, Peter Dadam*
Anwendungsspezifische Anforderungen an Workflow-Mangement-Systeme am Beispiel der Domäne Concurrent-Engineering

96-05 *Gerhard Schellhorn, Wolfgang Ahrendt*
Verification of a Prolog Compiler - First Steps with KIV

96-06 *Manindra Agrawal, Thomas Thierauf*
Satisfiability Problems

96-07 *Vikraman Arvind, Jacobo Torán*
A nonadaptive NC Checker for Permutation Group Intersection

96-08 *David Cyrluk, Oliver Möller, Harald Rueß*
An Efficient Decision Procedure for a Theory of Fix-Sized Bitvectors with Composition and Extraction

96-09 *Bernd Biechele, Dietmar Ernst, Frank Houdek, Joachim Schmid, Wolfram Schulte*
Erfahrungen bei der Modellierung eingebetteter Systeme mit verschiedenen SA/RT–Ansätzen

96-10 *Falk Bartels, Axel Dold, Friedrich W. von Henke, Holger Pfeifer, Harald Rueß*
Formalizing Fixed-Point Theory in PVS

96-11 *Axel Dold, Friedrich W. von Henke, Holger Pfeifer, Harald Rueß*
Mechanized Semantics of Simple Imperative Programming Constructs

96-12 *Axel Dold, Friedrich W. von Henke, Holger Pfeifer, Harald Rueß*
Generic Compilation Schemes for Simple Programming Constructs

96-13 *Klaus Achatz, Helmuth Partsch*
From Descriptive Specifications to Operational ones: A Powerful Transformation Rule, its Applications and Variants

97-01 *Jochen Messner*
Pattern Matching in Trace Monoids

97-02 *Wolfgang Lindner, Rainer Schuler*
A Small Span Theorem within P

97-03 *Thomas Bauer, Peter Dadam*
A Distributed Execution Environment for Large-Scale Workflow Management Systems with Subnets and Server Migration

97-04 *Christian Heinlein, Peter Dadam*
Interaction Expressions - A Powerful Formalism for Describing Inter-Workflow Dependencies

97-05 *Vikraman Arvind, Johannes Köbler*
On Pseudorandomness and Resource-Bounded Measure

97-06 *Gerhard Partsch*
Punkt-zu-Punkt- und Mehrpunkt-basierende LAN-Integrationsstrategien für den digitalen Mobilfunkstandard DECT

97-07 *Manfred Reichert, Peter Dadam*
$ADEPT_{flex}$ - Supporting Dynamic Changes of Workflows Without Loosing Control

97-08 *Hans Braxmeier, Dietmar Ernst, Andrea Mößle, Heiko Vogler*
The Project NoName - A functional programming language with its development environment

97-09 *Christian Heinlein*
Grundlagen von Interaktionsausdrücken

97-10 *Christian Heinlein*
Graphische Repräsentation von Interaktionsausdrücken

97-11 *Christian Heinlein*
Sprachtheoretische Semantik von Interaktionsausdrücken

97-12 *Gerhard Schellhorn, Wolfgang Reif*
Proving Properties of Finite Enumerations: A Problem Set for Automated Theorem Provers

97-13 *Dietmar Ernst, Frank Houdek, Wolfram Schulte, Thilo Schwinn*
Experimenteller Vergleich statischer und dynamischer Softwareprüfung für eingebettete Systeme

97-14 *Wolfgang Reif, Gerhard Schellhorn*
Theorem Proving in Large Theories

97-15 *Thomas Wennekers*
Asymptotik rekurrenter neuronaler Netze mit zufälligen Kopplungen

97-16 *Peter Dadam, Klaus Kuhn, Manfred Reichert*
Clinical Workflows - The Killer Application for Process-oriented Information Systems?

97-17 *Mohammad Ali Livani, Jörg Kaiser*
EDF Consensus on CAN Bus Access in Dynamic Real-Time Applications

97-18 *Johannes Köbler, Rainer Schuler*
Using Efficient Average-Case Algorithms to Collapse Worst-Case Complexity Classes

98-01 *Daniela Damm, Lutz Claes, Friedrich W. von Henke, Alexander Seitz, Adelinde Uhrmacher, Steffen Wolf*
Ein fallbasiertes System für die Interpretation von Literatur zur Knochenheilung

98-02 *Thomas Bauer, Peter Dadam*
Architekturen für skalierbare Workflow-Management-Systeme - Klassifikation und Analyse

98-03 *Marko Luther, Martin Strecker*
A guided tour through *Typelab*

98-04 *Heiko Neumann, Luiz Pessoa*
Visual Filling-in and Surface Property Reconstruction

98-05 *Ercüment Canver*
Formal Verification of a Coordinated Atomic Action Based Design

98-06 *Andreas Küchler*
On the Correspondence between Neural Folding Architectures and Tree Automata

98-07 *Heiko Neumann, Thorsten Hansen, Luiz Pessoa*
Interaction of ON and OFF Pathways for Visual Contrast Measurement